

EEG Analysis Based on Graph Spectral Theory

Zhaojin Chen

Department of Neurology and Neurosurgery

McGill University, Montreal, Canada

April 15, 2024

A thesis submitted to McGill University
in partial fulfillment of the requirements of the degree of Master of Science

ACKNOWLEDGEMENTS

Through the two years of postgraduate study, I have gained and grown a lot from my research, which could not have been achieved without the support of my family and friends and the help of my tutors.

My sincere appreciation to my supervisors, Prof. Amir Shmuel and Prof. Peng Xu, for guidance, and support towards my training and research development. They were always able to give me new ideas in my research like a lighthouse, always illuminating the road ahead.

Many thanks to my lab mates and friends: Li Cunbo, Chen Chunli, Jiang Lin, and other friends in the lab for discussions on my research and offering advice.

I would like to give special thanks to my parents, my brother, and Zhou Zixiong for all the support they have provided over the past three years. They always respect my choices, help me to digest the negativity, and are like a refueling station and a safe haven for me on the road ahead.

Numerous thanks to my committee member, Sue Ann Campbell, Pouya Bashivan, and my mentor Etienne De Villers-Sidani. Their expertise and wise advice were extremely valuable

ABSTRACT

The brain contains multiple cognitive processing subsystems. These subsystems are also known as brain regions which make up the complex network system--brain. Graph spectral theory, as an emerging technology to effectively mine the potential patterns of graph signals, has gradually become an important means of complex network analysis. A series of brain network analysis and information extraction methods have been developed based on graph spectral theory. These methods have been applied in brain signal processing (denoising), brain state assessment (brain disease diagnosis and treatment), etc. To further explore the capacity of graph spectral theory in the analysis and applications in the domain of brain signals, we focus on EEG denoising and the assessment of brain states. The specific research content of this thesis is as follows:

1. Research on EEG denoising techniques based on graph spectral theory. In this section, considering the high temporal and low spatial resolution of EEG signals, we construct a Joint-time Fourier Transform (JFT) filter based on the temporal and spatial smoothing constraints to address EEG denoising. To validate the robustness and effectiveness of the proposed JFT graph filtering method, we carry out simulation experiments and classification experiments with real EEG data. Wavelet and the JFT algorithm are compared. In the simulation experiments, we set up three types of noise for simulations of the noise associated with EEG acquisition. The results of the simulation experiments show that JFT is capable of suppressing different noise types better than the traditional algorithms and better than separate spatial smoothing filters and temporal smoothing filters. In the application experiments of real EEG signals, we use data from the P300 to validate the proposed JFT filtering method. The experimental results show that the accuracy of classification to schizophrenia with auditory hallucinations and healthy controls using the signal following denoising by the JFT algorithm is improved by 15%-30% compared with the classification before preprocessing, which demonstrates that JFT can effectively improve the decoding accuracy of EEG. Therefore, simulation experiments and real EEG application experiments show that the model can effectively suppress noise, achieve efficient EEG signal processing and robust component extraction, and provide effective technical support for future research on the development of EEG denoising technology.

2. Analysis of schizophrenia based on graph spectral theory. Based on the above studies, we further applied the connectome-harmonic decomposition (CHD) method developed from graph spectral theory to characterize the coupling of functional signals and structural networks in schizophrenia, to explore the changes in the dynamics of brain networks in schizophrenia and their links with neurocognitive changes. Specifically, we first found that scores on all neurocognitive tasks were lower in Schizophrenia (SCZ) patients compared to healthy controls. Then, to explore the electrophysiological abnormalities of SCZ patients and their association with neurocognitive changes, we first analyzed the scalp ERP and found that the P300 amplitude of SCZ patients showed a significant decrease compared to healthy controls. The results of the study showed that the total Graph Power Spectral Density (GPSD) of all harmonics in the SCZ patients was significantly reduced compared to the healthy controls and highly correlated with the neurocognitive scores. Then, considering that the low-frequency and high-frequency distributions of the graph harmonics correspond to the brain's two information processing mechanisms of functional integration and separation, we further classified the harmonic components into 10 sets from low to high. The results revealed that the energy of the 10 sets of harmonics was significantly lower in the SCZ patients compared to the healthy controls. In addition, to further investigate the relationship between graph harmonics and EEG rhythms, we designed graph filters based on the harmonic energies and filtered the signals into graph low-frequency aligned signals (captured by the first 4 harmonics) and graph high-frequency liberal signals (which are captured by the last 196 harmonics). Aligned signals are constrained by the structural graph while liberal signals are less constrained by the graph than aligned signals and are more liberal to change relative to the graph structure. The results of this study showed that the graph low-frequency aligned signals could effectively capture most of the different features of EEG rhythm between the two groups. In particular, the δ band in the graph low-frequency aligned signal effectively captured the abnormal activation of SCZ patients in prefrontal, temporal, and occipital regions. Correlation analysis demonstrated that the power spectral density of the δ band showed a positive correlation with cognitive ability and effectively predicted the neurocognitive task scores of the two groups. The above series of findings suggest that there are abnormal brain dynamics changes in SCZ during P300 which is highly correlated with its cognitive alterations. These results support the understanding of the neural mechanisms underlying changes in SCZ and provide new directions for its clinical

diagnosis, identification, and treatment. The demonstration that low-frequency graph harmonics capture most of the EEG rhythm indicates the reliability of low-frequency graph filters for EEG denoising and the possibility of applying graph harmonics for dimensionality reduction.

Keywords: Graph Spectral Theory, EEG Denoising, Schizophrenia, Connectome-Harmonic Decomposition, Graph Signal Processing

RÉSUMÉ

Le cerveau contient plusieurs sous-systèmes de traitement cognitif. Ces sous-systèmes sont également connus sous le nom de régions cérébrales qui composent le système de réseau complexe - le cerveau. La théorie spectrale des graphes, en tant que technologie émergente pour exploiter efficacement les motifs potentiels des signaux de graphes, est progressivement devenue un moyen important d'analyse des réseaux complexes. Une série de méthodes d'analyse du réseau cérébral et d'extraction d'informations ont été développées sur la base de la théorie spectrale des graphes. Ces méthodes ont été appliquées dans le traitement des signaux cérébraux (débruitage), l'évaluation de l'état cérébral (diagnostic et traitement des maladies cérébrales), etc. Pour explorer davantage la capacité de la théorie spectrale des graphes dans l'analyse et les applications dans le domaine des signaux cérébraux, nous nous concentrons sur le débruitage de l'EEG et l'évaluation des états cérébraux. Le contenu de recherche spécifique de cette thèse est le suivant :

1. Recherche sur les techniques de débruitage de l'EEG basées sur la théorie spectrale des graphes. Dans cette section, compte tenu de la haute résolution temporelle et de la faible résolution spatiale des signaux EEG, nous construisons un filtre de transformée de Fourier temporelle commune (JFT) basé sur les contraintes de lissage temporel et spatial pour résoudre le débruitage de l'EEG. Pour valider la robustesse et l'efficacité de la méthode de filtrage de graphe JFT proposée, nous menons des expériences de simulation et des expériences de classification avec des données EEG réelles. L'ondelette et l'algorithme JFT sont comparés. Dans les expériences de simulation, nous configurons trois types de bruit pour simuler le bruit associé à l'acquisition EEG. Les résultats des expériences de simulation montrent que JFT est capable de supprimer différents types de bruit mieux que les algorithmes traditionnels et mieux que les filtres de lissage spatial et temporel séparés. Dans les expériences d'application des signaux EEG réels, nous utilisons des données du P300 pour valider la méthode de filtrage JFT proposée. Les résultats expérimentaux montrent que la précision de la classification de la schizophrénie avec hallucinations auditives et de sujets témoins en bonne santé en utilisant le signal après débruitage par l'algorithme JFT est améliorée de 15 % à 30 % par rapport à la classification avant prétraitement, ce qui démontre que JFT peut améliorer efficacement la précision de décodage de l'EEG. Par conséquent, les expériences de simulation et les

expériences d'application EEG réelles montrent que le modèle peut supprimer efficacement le bruit, réaliser un traitement efficace des signaux EEG et une extraction robuste des composantes, et fournir un support technique efficace pour les futures recherches sur le développement de la technologie de débruitage de l'EEG.

2. Analyse de la schizophrénie basée sur la théorie spectrale des graphes. Sur la base des études ci-dessus, nous avons appliqué la méthode de décomposition harmonique du connectome (CHD) développée à partir de la théorie spectrale des graphes pour caractériser le couplage des signaux fonctionnels et des réseaux structuraux dans la schizophrénie, pour explorer les changements dans la dynamique des réseaux cérébraux dans la schizophrénie et leurs liens avec les changements neurocognitifs. Plus précisément, nous avons d'abord constaté que les scores sur toutes les tâches neurocognitives étaient plus bas chez les schizophrènes (SCZ) par rapport aux sujets témoins en bonne santé. Ensuite, pour explorer les anomalies électrophysiologiques de la SCZ et leur association avec les changements neurocognitifs, nous avons d'abord analysé l'ERP du cuir chevelu et avons constaté que l'amplitude du P300 de la SCZ présentait une diminution significative par rapport aux sujets témoins en bonne santé. Les résultats de l'étude ont montré que la densité spectrale de puissance graphique totale (GPSD) de toutes les harmoniques dans la SCZ était significativement réduite par rapport aux sujets témoins en bonne santé et hautement corrélée avec les scores neurocognitifs. Ensuite, considérant que les distributions de basses et hautes fréquences des harmoniques du graphe correspondent aux deux mécanismes de traitement de l'information cérébrale d'intégration fonctionnelle et de séparation, nous avons ensuite classé les composantes harmoniques en 10 ensembles de bas en haut. Les résultats ont révélé que l'énergie des 10 ensembles d'harmoniques était significativement plus faible dans la SCZ par rapport aux sujets témoins en bonne santé. De plus, pour enquêter davantage sur la relation entre les harmoniques du graphe et les rythmes EEG, nous avons conçu des filtres de graphe basés sur les énergies harmoniques et filtré les signaux en signaux alignés de basse fréquence du graphe (capturés par les 4 premières harmoniques) et signaux libéraux de haute fréquence du graphe (capturés par les 196 dernières harmoniques). Les signaux alignés sont contraints par le graphe structurel tandis que les signaux libéraux sont moins contraints par le graphe que les signaux alignés et sont plus libéraux pour changer par rapport à la structure du graphe. Les résultats de cette étude ont montré que les signaux alignés de basse fréquence du graphe pouvaient capturer efficacement la plupart des

caractéristiques différentes du rythme EEG entre les deux groupes. En particulier, la bande δ dans le signal aligné de basse fréquence du graphe capturait efficacement l'activation anormale de la SCZ dans les régions préfrontales, temporales et occipitales. L'analyse de corrélation a démontré que la densité spectrale de puissance de la bande δ présentait une corrélation positive avec la capacité cognitive et prédisait efficacement les scores des tâches neurocognitives des deux groupes. L'ensemble de ces résultats suggère qu'il existe des changements anormaux dans la dynamique cérébrale de la SCZ pendant le P300 qui sont fortement corrélés avec ses altérations cognitives. Ces résultats soutiennent la compréhension des mécanismes neuronaux sous-jacents aux changements de la SCZ et fournissent de nouvelles orientations pour son diagnostic clinique, son identification et son traitement. La démonstration que les harmoniques graphiques de basse fréquence capturent la plupart du rythme EEG indique la fiabilité des filtres de graphe de basse fréquence pour le débruitage de l'EEG et la possibilité d'appliquer les harmoniques du graphe pour la réduction de dimension.

Mots-clés: Théorie spectrale des graphes, Débruitage de l'EEG, Schizophrénie, Décomposition harmonique du connectome, Traitement des signaux graphiques

Table of Contents

Table of Contents

Chapter 1	Introduction	1
1.1	Background and Significance of this Research	1
1.2	EEG and Its Applications	2
1.3	Graph Spectral Theory and Its Application to Brain Science	4
1.3.1	Brain Network	5
1.3.2	Connectome-Harmonic Decomposition Analysis	6
1.3.3	Denoising	8
1.4	Related Studies	10
1.4.1	Overview of Noise in EEG and Current Denoising Algorithms	10
1.4.2	Schizophrenia	13
1.5	The Main Contributions of this Thesis	18
1.6	Organization of the Thesis	20
Chapter 2	JFT Filter for EEG Denoising Based on Graph Spectral Theory	21
2.1	Abstract	21
2.2	Introduction	22
2.3	JFT Graph Filter	24
2.3.1	The Basics of Graph Spectral Theory	24
2.3.2	Joint Time-vertex Framework	26
2.3.3	Graph Smoothing Filter Based on the l_{pq} norm	27
2.3.4	Stepwise Linear Discriminant Analysis	30
2.4	Simulation and Real Data Classification Results	31
2.4.1	Dataset	31
2.4.2	Simulation Noise and Simulation Results	32
2.4.3	Classification Results	37
2.5	Discussion	38
2.6	Conclusion	41
Chapter 3	Analysis of Schizophrenia Based on Graph Spectral Theory	42
3.1	Abstract	42
3.2	Introduction	43
3.3	Data and Processing Flow	45

Table of Contents

3.3.1 Data	45
3.3.2 Data Processing Flow	45
3.4 Methods	47
3.4.1 Source Localization Techniques	47
3.4.2 Construction of Consensus Structural Brain Networks	48
3.4.3 Graph Power Spectral Density	49
3.4.4 Power Spectral Density	50
3.4.5 Correlation and Regression Prediction Analysis	51
3.5 Results	52
3.5.1 Cognitive Scales and ERPs	52
3.5.2 GPSD	53
3.5.3 Correlation and Prediction Results	55
3.6 Discussion	58
3.7 Conclusion	61
Chapter 4 General discussion	63
4.1 Key Findings and Significance	63
4.2 Future Research	65
Chapter 5 Bibliography	67

Chapter 1 Introduction

1.1 Background and Significance of this Research

Electroencephalogram (EEG) is a reliable, non-invasive acquisition of brain activity that effectively captures the electrophysiological activity of the brain. Compared to functional and structural magnetic resonance imaging, EEG signals are inexpensive, convenient, and easy to obtain. In addition, a large amount of psychological and disease information is contained in EEG signals. Therefore, in recent years, there have been more and more cognitive and disease studies based on EEG. For example, EEG is widely used in human sleep state detection, motor imagery, decision-making, and other studies(Gaur et al., 2021; Markovic, Kaess, & Tarokh, 2020; Si et al., 2020).

However, EEG is highly susceptible to the interference of noise signals during the acquisition process. This will greatly affect the decoding efficiency and accuracy of EEG and the establishment of computational models for disease diagnosis. Traditional algorithms for EEG denoising mainly include blind source estimation and wavelet transform(Carmona & Hudgins, 1994; De Clercq, Vergult, Vanrumste, Van Paesschen, & Van Huffel, 2006; Makeig, Bell, Jung, & Sejnowski, 1995). The blind source analysis method mainly treats the EEG as a linear weighted sum of various independent sources. Because of the different distribution patterns of the noise and the signal, the noise source is eliminated to achieve the purpose of noise removal. On the other hand, wavelet transform mainly filters out noise signals by threshold selection methods, because the amplitudes for wavelet coefficients of noise are small and more dispersed compared with those of signals after wavelet transform. However, these existing methods ignore the fact that as a highly connected system, the brain has interdependence between its different channels, which may affect the performance of these denoising algorithms.

In addition, cognitive processes are always accompanied by synchronized activation between local or global neurons, suggesting that cognitive processes involve synergistic functioning and information transfer between different regions of the brain. Therefore, separate time-frequency domain approaches are not sufficient to decode how synchronized activity in brain regions is involved in cognitive activities. For this reason, many studies have considered EEG signals as graph signals and analyzed the features of EEG signals in terms of graph features. To explore the information interaction patterns

between different brain regions in different cognitive tasks, complex network methods have been used to extract the features of EEG signals. For example, linear methods such as Coherence (COH), Phase Locking Value (PLV), and dynamic nonlinear models such as Granger Causality Analysis (GCA) have been used to characterize the functional connectivity of the brain in EEG studies (Basharpoor, Heidari, & Molavi, 2021; Dongwei, Fang, Zhen, Haifang, & Junjie, 2013; Z.-M. Wang, Zhou, He, & Guo, 2020). These algorithms are widely used in disease and cognitive studies to provide corresponding quantitative criteria for the interaction patterns between different brain regions and provide explanations of the neural mechanisms for brain diseases and specific cognitive states. However, these studies based on graph theory mainly focus on structural and functional connections, ignoring the coupling characteristics between functional signals and structural connections.

Therefore, this thesis develops denoising algorithms for EEG signals as well as feature extraction techniques based on graph spectral theory. Then, the above algorithms were applied to the denoising of P300 signals and the coupled feature between functional signals and structural networks in schizophrenia. These algorithms will contribute to the future development of EEG denoising technology and characteristic exploitation of disease and cognition, and promote the practical application of brain science in related fields such as neural engineering and clinical cognitive diagnosis.

1.2 EEG and Its Applications

Electrophysiological activities of the brain present different rhythmic distributions in different cognitive states. EEG rhythms provide valuable information for us to explore the cognitive functions of the brain and diagnosis methods of brain diseases. These rhythms are mainly classified according to their frequency and amplitude, and the following is a basic introduction of the 5 rhythms in EEG:

Delta waves (1-4Hz). Compared to other waves, delta waves are large in amplitude and fluctuate slowly. This rhythm is commonly associated with deep sleep, immature brains in infants, and some brain disorders. For example, abnormal δ waves can be observed in the brains of patients suffering from sleep apnoea, or brain injury, or in the brains of epileptic patients during their slow-wave sleep (Amzica & Steriade, 1998; Ferrillo, Beelke, & Nobili, 2000; Tarokh, Carskadon, & Achermann, 2010).

Theta waves (4-8 Hz). Theta waves fluctuate more rapidly than δ waves and are usually seen in drowsiness, meditation, and Rapid Eye Movement (REM) sleep. In addition to this, theta waves play an important role in memory formation and learning processes (Buzsáki, 2002).

Alpha waves (8-13 Hz). Alpha wave is prominent when the brain is awake and relaxed with eyes closed. It is often thought to be associated with an idle state of the brain, especially a relaxed but alert mental state.

Beta waves (13-30 Hz). Beta waves occur when the brain is alert, thinking actively, and concentrating.

Gamma waves (30Hz-100Hz). Gamma waves are the fastest fluctuating waves among these five rhythms and are mainly involved in cognitive processes such as attention, memory, and perception.

In addition, EEG can also be classified into spontaneous EEG and evoked EEG according to the presence or absence of external stimuli or tasks. Spontaneous EEG refers to the electrophysiological activity generated spontaneously by the brain in the absence of any external stimulus or task and it responds to the basic state and function of the brain. Spontaneous EEG is also closely related to an individual's cognitive function and attention level. Evoked EEG, on the other hand, refers to the electrophysiological activity of the brain induced by specific stimuli or tasks. Evoked EEG is important for the study of specific perceptual and cognitive processes, circuit abnormalities in neurological disorders, and modern brain-computer interfaces. For example, some patients with schizophrenia experience symptoms such as hallucinations. Wang et al. found that schizophrenic patients without auditory hallucinations were found to have relatively stronger connectivity in the left frontal and posterior parietal lobes through the evoked P300 signal by the auditory oddball stimuli (J. Wang et al., 2023). In addition to this, many applications of brain-computer interfaces are carried out precisely with the help of evoked EEG. For example, in motor rehabilitation, patients are given a specific motor task and their brain signals are captured and analyzed in real-time (Hobbs & Artemiadis, 2020; Morone et al., 2017). After the task is presented, the patients control their brain activities through intention. Then their brain signals are recorded, decoded, translated into corresponding commands, and sent to devices such as prosthetic limbs or exoskeletons. Finally, the patient can observe the real-time feedback and make self-adjustments to facilitate the repair of their damaged limb. In addition, the P300-based spelling system

may in the future provide a robust spelling strategy for every motor-disabled patient, so that they can enjoy chatting on the Internet through their mind as well.

In conclusion, EEG has high temporal resolution and can provide rich brain information for real-time decoding of brain states during cognitive processes. Besides, the rich rhythmic information of EEG also provides a basis for the exploration and diagnosis of cognitive functions and diseases. These advantages make EEG widely used in brain-computer interface and exploration of cognitive functions and diseases. On the one hand, the development of EEG network dynamics techniques helps us to further understand and explore cognitive abnormalities in patients with brain diseases, and thus develop effective treatments and interventions. On the other hand, noise can greatly interfere with the performance of computational models for disease diagnosis and brain-computer interfaces in EEG, and thus the development of robust noise suppression strategies remains very promising and important.

1.3 Graph Spectral Theory and Its Application to Brain Science

Graph spectral theory is commonly used in computer science and information computing, mainly for the study of the properties and structure of graphs. In this theory, a graph is represented as a collection of nodes and edges connecting these nodes. The main idea of graph spectral theory is to consider the graph as a matrix, then construct the Laplace matrix of the graph, and study the structure and characteristics of the graph by some mathematical operations such as eigenvalue decomposition of the Laplace matrix. In brain science, graph spectral theory is widely used in brain network analysis, classification, and denoising of functional signals. However, compared to functional network approaches, harmonic analysis techniques and denoising algorithms developed by graph spectral theory have been used less in EEG analysis. To address this, this thesis develops corresponding algorithms, aiming to provide new insight for the future development of EEG denoising techniques and further understanding of cognitive impairment mechanisms for psychiatric disorders from the perspective of network dynamics. In the next section, this thesis will focus on the application of graph spectral theory in brain science.

1.3.1 Brain Network

Brain activity involves interactions and coordination among multiple brain regions, and the information interactions among these brain regions can be portrayed by the complex network. When applying the complex network to brain science, we usually consider individual brain regions as individual nodes in a graph, and the connected edges quantify the distances or the closeness between the nodes. Currently, graph theory is widely used in brain network studies of cognitive, psychiatric, or neurological disorders of the brain.

To construct structural networks with Diffusion Tensor Image (DTI), firstly, the ROIs as nodes on the graph are divided according to the template. The direction model is then used to estimate the fiber and diffusion direction within the discrete voxels. Then, according to the bundle imaging algorithm, the approximate fiber bundles of the streamlines are obtained. Finally, the number of streamlines can be obtained to construct the adjacency matrix. Meanwhile, the construction method of functional connectivity is much easier compared to structural connectivity. The ROI is firstly determined based on the template, and the functional signals of individual ROIs are usually obtained by averaging the signal in the voxel of each ROI. Then, the coupling strength between two nodes is determined by algorithms like COH, PLV, and GCA (Basharpour et al., 2021; C. Li et al., 2023; P. Li et al., 2023), etc.

Brain networks provide evidence for the exploration of brain function and disease. An increasing number of studies have shown that many brain diseases can be regarded as disorders of brain networks. For example, several studies have reported abnormalities in the resting functional network of the brain in Parkinson's patients at the striatum (Hacker, Perlmutter, Criswell, Ances, & Snyder, 2012; Helmich et al., 2010). Gratton et al. found that the differences in resting-state functional connectivity in Parkinson's patients compared with healthy subjects were mainly in the sensorimotor, thalamic, and cerebellar networks (Gratton et al., 2019). In addition, Sonuga-Barke and Castellanos et al. proposed the "default mode interference" hypothesis, in which they suggested that abnormal behaviors in Attention Deficit Hyperactivity Disorder (ADHD) may be associated with synchronous dysfunction of the default network (Castellanos et al., 2008; Sonuga-Barke & Castellanos, 2007). With a working memory-related paradigm, researchers have found a significant increase in reaction time during working memory tasks in ADHD. They suggest that distraction in ADHD may be related to an inability to adequately inhibit

activity in the default network in response to increased task difficulty(Fassbender et al., 2009). Furthermore, cognitive deficits in Autism Spectral Disorder (ASD) may be due to a widespread lack of connectivity to brain regions relevant for information integration. In support of this hypothesis, several studies have reported deficits in connectivity of task-related brain regions for ASD(Just, Cherkassky, Keller, Kana, & Minshew, 2007; Kana, Keller, Cherkassky, Minshew, & Just, 2006; Rudie et al., 2012). In addition to this, disruptions in anatomical and functional connectivity in the frontal and temporal lobes in schizophrenia have been commonly reported (Price et al., 2008) (Zalesky, Fornito, & Bullmore, 2010). In addition, brain networks have been used in emotional brain-computer interfaces(Dongwei et al., 2013) and ASD diagnosis (Light et al., 2006).

1.3.2 Connectome-Harmonic Decomposition Analysis

The above studies demonstrate that brain networks provide richer information about brain interactions. However, it can't reveal how functional signals are generated from the rich structural networks. Thus, it is necessary to explore new network dynamics techniques for further exploration and explanation of this part of the study. To solve this problem, the Connectome Harmonic Decomposition (CHD) method based on graph spectral theory has emerged.

Currently, CHD is commonly used for multimodal analysis of MRI and EEG. Usually, researchers use structural images to construct the adjacency matrix and then the Laplace matrix can be obtained. The eigenvectors of the Laplace matrix are then obtained by singular value decomposition, which is also known as connectivity harmonics. Connectivity harmonics are closely related to brain structure and cognitive tasks. Functional harmonics of dense functional connectivity reveal cortical structures and a small number of harmonics are sufficient to decode patterns of task activity(Glomb et al., 2021). CHD re-expresses functional signals primarily with their dependence on underlying structural connectivity(Luppi et al., 2023). Function signal can be represented as a weighted sum of a series of connectome harmonics that represent different spatial scales of brain activities. CHD emphasizes viewing brain activity from different spatial scale perspectives, quantifying the extent to which functional signals are constrained by or deviate from the global network of underlying structures. Based on the above theory, many studies have begun to explore the coupling features of functional signals and connectivity harmonics from the perspective of connectome harmonics.

With Functional Magnetic Resonance Imaging (fMRI) as a functional signal, Sihag et al. found that CHD features captured Neurofilament (NFL) levels in healthy controls and brain-injured patients. The changes in CHD features of brain-injured patients were independent of aging. Thus, this study demonstrates that NFL levels can be a reliable marker of brain damage to neural axons(Sihag et al., 2022). Luppi et al. explored how consciousness arises from a network of fixed anatomical connections with CHD(Luppi et al., 2023). They found that in both anesthetized healthy subjects and brain-injured patients, a trend towards increased energy of low-frequency connectivity harmonic and decreased energy of high-frequency connectome harmonics was observed during their loss of consciousness, while the opposite trend was found in induced psychedelic states. In another study, Atasoy investigated the cross-frequency correlations between brain harmonics and found that Lysergic Acid Diethylamide (LSD) significantly increased the cross-frequency correlations between different graph harmonics(Atasoy et al., 2017). In addition, Jiao et al. revealed a constrained relationship between blood oxygenation and glucose metabolism in the white matter of the human brain based on CHD(J. Li et al., 2023).

On the other hand, researchers have decomposed EEG onto connectome harmonics, allowing us to track changes in brain network dynamics at the millisecond level(Glomb et al., 2020). Glomb et al. found that 90% of the energy of the brain signal was captured by the smoothest low-frequency connectome harmonics based on CHD. Besides, a small number of connectome harmonics were sufficient to reproduce brain activity during a face detection task and they revealed patterns of co-activation in somatosensory and frontal cortex in the task(Glomb et al., 2020). Rué-Queralt then compared the effects of Principal Component Analysis (PCA), Independent Component Analysis (ICA), and CHD on the dimensionality reduction of functional signals. They found that CHD can more compactly represent functional signals and distributed functional activities in the cerebral cortex tended to appear more in the alpha, theta, and other frequency bands, whereas local brain activities tended to appear in the gamma frequency band(Rué-Queralt et al., 2021; Rué-Queralt et al., 2023).

The above study explains the characteristics of functional signals coupled with structural networks and provides a basis for the study of spatio-temporal dynamics of the brain based on CHD. Besides, CHD has also been used in feature extraction and classification. Saboksayr applied Graph Signal Processing(GSP) learning to the

construction of functional brain connectivity of EEG and analyzed the graph harmonics of different emotional states. They found that the frontal energy of low-valence in the low-frequency graph harmonics showed an asymmetric distribution, which is in line with the present study and two types of emotional states can be classified with an accuracy rate of 92.73% by the low-frequency graph harmonics(Saboksayr, Mateos, & Cetin, 2021). Georgiadis et al. investigated the graph harmonic features of cross-frequency coupling networks and used them in the classification of motor imagery EEG. They achieved better results than conventional methods like Common Spatial Pattern (CSP) (K Georgiadis, Laskaris, Nikolopoulos, & Kompatsiaris, 2019). Petrovic proposed the graph Slepian operator to solve the problem of signal energy concentration in some nodes and some graph domains (Petrovic, Bolton, Preti, Liégeois, & Van De Ville, 2019). Based on this, Georgiadis improved the original recognition algorithm to achieve higher classification accuracy(Kostas Georgiadis, Adamos, Nikolopoulos, Laskaris, & Kompatsiaris, 2021).

Overall, the above studies illustrate that CHD provides a robust strategy for feature extraction that captures the corresponding cognition and disease features, potentially providing a new way of constructing diagnostic models for diseases. However, few studies have been carried out on this aspect in the study of schizophrenia. Based on this, this thesis proposes a feature extraction method for schizophrenia based on the DTI consensus structural network to investigate the coupling characteristics of structural networks and functional signals in schizophrenia. This study may provide some new insight into the neural mechanisms of cognitive disorders in schizophrenia.

1.3.3 Denoising

For the denoising of functional signals, Graph Signal Processing (GSP) developed from graph spectral theory provides techniques for graph signal filtering. The low frequency of the graph captures the global connectivity patterns and most of the energy of the signals. Thus, a low-pass graph filter achieves denoising by preserving the low-dimensional harmonics and thus preserving the relative invariance of the global connectivity between nodes. This domain-smoothing filter based on the underlying graph structure is not considered by previously proposed conventional denoising algorithms. Thus, in the field of brain science, more researchers have started to apply graph filters based on the underlying graph structure to denoise functional signals.

In FMRI studies, researchers found that the white matter Blood Oxygen Level Dependent (BOLD) signal has a consistent spatial correlation structure with the water diffusion direction measured by DTI, which suggests that the white matter BOLD signal has a strong dependence on the anatomical structure. Based on this, Abramian et al. introduced GSP into the spatial smoothing of white matter BOLD signals for the first time and designed a DSS technique for domain-informed smoothing, which was found to be superior to the isotropic Gaussian filters commonly used for functional signal smoothing(Abramian et al., 2021). Behjad exploited the topological constraints provided by grey-white and cortical surfaces to perform a smoothing operation on cortical fMRI in volume space, making the filtering process more attuned to the details of the underlying brain morphology and structure(Behjat, Westin, & Aganj, 2021).

Besides, graph spectral theory has been increasingly used in EEG denoising. Pentari et al. proposed a new method based on the GSP technique to suppress the effect of heavy tail noise in EEG and verified the effectiveness of this algorithm in epileptic EEG denoising(Pentari, Tzagkarakis, Marias, & Tsakalides, 2021, 2022). Wenqiang et al. regarded EEG as an image and applied the graph filtering method to denoise EEG signal to improve the efficiency of the brain-computer interface based on Steady-state Visual Evoked Potentials (SSVEP)(Yan, Du, Wu, Zheng, & Xu, 2021). Einizadet solved the problem of blind source separation and designed the GraDe method by assuming that each source has a unique graph and temporal connectivity structure for a short period (Einizade & Sardouie, 2022).

Graph spectral theory can retain the constraints between channels or brain regions rather than previous algorithms. Thus, it may be more adapted to the structural features of the brain itself. So, it may be one of the focuses of EEG denoising research in the future. Compared with signals such as communication signals, EEG signals are concentrated in low frequency bands and the overall changes are smoother. In addition, compared to functional signals such as FMRI, the spatial resolution of EEG is low and the temporal resolution is high, and thus individual spatial filtering algorithms may not be able to cope with complex noise. Therefore, unlike previous studies, we achieve denoising of EEG signals with the joint temporal and spatial smoothness constraints mainly based on graph spectral theory. This framework may be able to better cope with complex acquisition noise than traditional methods

1.4 Related Studies

In this study, we mainly focus on graph spectral theory for EEG denoising and the neural mechanisms of cognitive deficits for schizophrenia based on CHD. Therefore, this section will focus on these two aspects to introduce the current EEG denoising techniques as well as related research on schizophrenia.

1.4.1 Overview of Noise in EEG and Current Denoising Algorithms

The brain is a special interconnected structure with noise interference between acquisition channels. Besides, during signal collection, EEG is susceptible to environmental noise, acquisition system noise, and so on. Designing a robust filter to obtain artifact-free EEG signals is both a challenge and an opportunity. This section will focus on the sources of noise and the current research on denoising algorithms.

EEG originates from the synchronized firing activity of millions of neurons. The generated electrical impulses can be detected by electrodes placed on the scalp. During the acquisition process, various noises can distort EEG. The main sources of these noises are as follows:

- 1) From the acquisition equipment. EEG signals are very weak and the acquired signals need to be amplified by an amplifier to be captured. During this process, thermal noise is introduced by the acquisition device.
- 2) From electromagnetic interference. The most common noise is Industrial Frequency Interference (IFI) in the frequency range of 50 Hz-60 Hz.
- 3) From the electrodes. On the one hand, poor contact with the scalp or loosening of the electrode can introduce noise and lead to distortion of EEG waveforms; on the other hand, poor quality of electrodes can also lead to artifacts.
- 4) From various physiological activities of the human body, especially the interference generated by muscle movements, such as electrooculography, electromyography, and electrocardiogram.

EEG denoising technology plays an important role in the analysis of brain cognition and disease. Effective EEG denoising technology can greatly improve the accuracy of disease diagnosis and help to accurately capture brain functional activation patterns.

Hans Berger first recorded EEG waves through electrodes in 1924 and put forward his insights for feature extraction and denoising of EEG signals, which provided a reliable basis for subsequent EEG signal research (La Vaque, 1999). After that, the Fourier

transform and Wiener filter were gradually used in the denoising of EEG signals(Borowicz, 2018; Carlton & Katz, 1980). A Wiener filter is designed from the frequency domain, which mainly targets one-dimensional non-smooth signals. Since EEG is a non-stationary signal, the application of Wiener filtering has some drawbacks. After that, the Kalman filter was proposed in 1960, which can handle both stationary and non-stationary random signals. Then Bohlin used the Kalman filter to denoise EEG for the first time(Bohlin, 1977).

In recent years, blind source analysis techniques such as ICA and Canonical Correlation Analysis (CCA), wavelet transform, deep learning, graph learning, and other new methods have been applied in EEG denoising, which has favorably promoted the development of EEG denoising algorithms.

In blind source analysis, ICA linearly decomposes multichannel EEG into maximally statistically independent components by utilizing Higher-Order Statistics (HOS)(Makeig et al., 1995). With Second-Order Statistics (SOS), CCA uses the original EEG as the first dataset and its delayed version as the second dataset, aiming to find maximally autocorrelated and mutually uncorrelated sources(De Clercq et al., 2006). The denoising of ICA mainly takes advantage of the fact that the distribution of noise has significant features, e.g., the topography of electrooculographic artifacts is mainly located at the front eye electrodes, and the power spectral curve of this component does not have any obvious mutation points. CCA takes advantage of the feature that the autocorrelation of muscle artifacts is relatively low compared to brain activity. Makeig first used ICA in EEG denoising, and Hyvärinen and Sardouie improved on the original ICA technique and proposed Fast-ICA and Jacobi-like ICA algorithms(Hyvärinen & Oja, 1997; Makeig et al., 1995; Sardouie, Albera, Shamsollahi, & Merlet, 2014). Clercq first applied CCA to noise removal of EEG signals(De Clercq et al., 2006).

As the most effective time-frequency analysis method, Wavelet Transform (WT) is mainly used to decompose the signal onto wavelets of different time-frequency scales. After this transformation, most of the energy of the EEG signal will be concentrated in a few larger wavelet coefficients. Through the threshold selection, we can remove the noise in the signal. Carmon applied the wavelet transform to de-noise the EEG signals in 1998(Carmona & Hudgins, 1994). After that, different solutions have been proposed by researchers for the selection of wavelet threshold. The most classical method was proposed by Donoho and Johnstone et al(Donoho & Johnstone, 1994, 1995). Besides,

there are various thresholding strategies such as hard thresholding and soft thresholding(Khatwani & Tiwari, 2013; Şendur & Selesnick, 2002). In general, soft thresholding outperforms hard thresholding methods for denoising. Alyasseri et al. compared different meta-optimization methods for the selection of wavelet thresholds, and finally found that the Flower Pollination Algorithm (FPA) performed the best(Alyasseri, Khader, Al-Betar, Abasi, & Makhadmeh, 2019).

Subsequently, a large number of hybrid adjustable algorithms have been proposed. The wavelet transforms or Multimodal Experience Modeling decomposition (MEMD) combined with CCA can enhance the algorithm's ability to suppress muscle artifact noise(Chen, Xu, Liu, McKeown, & Wang, 2017; Mowla, Ng, Zilany, & Paramesran, 2015). These algorithms utilize the autocorrelation of EEG signals in the time-frequency domain and the mutual uncorrelation between individual channels. They first decompose the signal by time-frequency methods and then reconstruct the artifact-free signal after CCA decomposition. In addition to this, Dora et al. proposed a technique to remove EEG artifacts with minimal supervision based on a data-driven approach(Dora & Holcman, 2022).

In addition to this, deep learning methods have been increasingly used in EEG denoising due to their good adaptability and performance. Haoming et al. provided a benchmark dataset that can be used for the training and testing of EEG denoising models and compared the denoising effects of different classical networks(Zhang et al., 2021). U-Net, GAN, and many other deep-learning strategies were applied to noise removal (An, Lam, & Ling, 2022; Chuang, Chang, Huang, & Jung, 2022; Mashhadi, Khuzani, Heidari, & Khaledyan, 2020). Chuang combined ICA and deep learning to reconstruct EEG signals, firstly separating the original signals by ICA, and then reconstructing the EEG signals by U-NET filtering(Chuang et al., 2022).

However, most of these methods, wavelet transform and deep learning do not take into account the interdependence between different brain regions or acquisition channels. Based on this, researchers propose new denoising methods based on graph signal processing techniques. Compared with previous algorithms, graph signal processing algorithms mainly rely on the constraints of the underlying structural graph.

In conclusion, denoising is of great significance in the brain-computer interface and the construction of cognition and disease models. It not only improves the signal quality of EEG but also enhances the signal characteristics and improves the performance of the

brain-computer interface. However, nowadays, the current algorithms mainly focus on the separate consideration of denoising from time-frequency and spatial aspects. Therefore, this thesis proposes the Joint-time vertex (JTV)(Grassi, Loukas, Perraudin, & Ricaud, 2017) framework to solve the denoising problem of EEG signals. The simultaneous temporal and spatial constraints may achieve superior noise reduction.

1.4.2 Schizophrenia

Schizophrenia (SCZ) is one of the most common psychiatric disorders and is usually characterized by disturbances in various aspects of emotion, behavior, consciousness, and perception. Patients usually suffer from hallucinations, delusions, disorganized speech, social withdrawal, and emotional apathy. These symptoms often seriously interfere with the patient's daily life, work, and study. Besides, these symptoms of schizophrenia can be further categorized into positive and negative symptoms. Positive symptoms of schizophrenia refer to patients who experience additional experiences and behaviors; negative symptoms refer to patients with schizophrenia who lack some of the emotions or behaviors that healthy people have.

As reported in the Global Burden of Disease Survey for Mental Disorders 2019, the SCZ global prevalence rate was 0.29%. Besides, schizophrenia increases the risk of death by two to three times(McGrath, Saha, Chant, & Welham, 2008). In addition, schizophrenia tends to be a lifelong illness that is not easily cured, thus causing a serious burden on patients and their families. Kane compared the effectiveness of comprehensive early treatment with that of usual community care for schizophrenia and found that those treated longer had greater improvements in quality of life and psychopathology, and were able to participate in more work and school learning(Kane et al., 2016). Thus, early diagnosis and treatment are essential for schizophrenia.

Currently, the diagnosis of schizophrenia is based on the subjective judgment of the physician, DSM-5 diagnostic criteria, and the patient's family history and symptoms. The DSM-5(Tandon et al., 2013) provides clear diagnostic criteria in symptomatology, duration, dysfunction, etc., which helps physicians to give an accurate classification of the diseases, thus facilitating subsequent pathologic and imaging research. However, schizophrenia is also prone to misdiagnosis due to various factors. For example, some of the symptoms of schizophrenia usually overlap with those of other mental disorders(Ayano et al., 2021). In addition, in the early stage of schizophrenia, the patient's

symptoms gradually appear but they may not cooperate with the doctor and conceal the actual symptoms when seeking medical treatment, causing a wrong diagnosis. Therefore, pathology, imaging, and EEG studies are beneficial to promote the objective diagnosis of schizophrenia, as well as important for the exploration of effective individualized treatments for schizophrenia.

In addition, diagnostic methods based on pathology, imaging, and EEG are still being explored, and they provide evidence for functional and structural abnormalities of schizophrenia. In the following section, the current research on schizophrenia will be introduced from the perspective of pathologic studies, imaging studies, and EEG.

1.4.2.1 Pathology Studies

Currently, research has found that a variety of proteins are abnormally expressed in the brains of schizophrenia, especially proteins associated with neurotransmitters. Abnormal expression of these neurotransmitters leads to disturbances in neuronal signals.

Among the causes of schizophrenia, the one that has received the most attention is the dopamine hypothesis. It suggests that abnormal activity of the dopamine system plays an important role in the pathogenesis of schizophrenia. An early study by Carlsson et al. found that the antipsychotic drug reserpine blocked the reuptake of dopamine and other monoamines (Carlsson & Lindqvist, 1963). After that, Lieberman et al. noted that sodium aniline increases synaptic monoamine levels and induces psychotic symptoms (Lieberman, Kane, & Alvir, 1987). At this time, researchers did not find a direct link between dopamine and schizophrenia. After the 1970s, researchers found a direct correlation between the effectiveness of these antipsychotic medications and the affinity of dopamine receptors (Creese, Burt, & Snyder, 1976; Seeman & Lee, 1975). Creese and Seeman, et al. suggested that these medications treated psychiatric illness primarily by blocking the over-reception of dopamine receptors (Creese et al., 1976; Seeman & Lee, 1975). Later, the researchers combined schizophrenia with genetics and neurodevelopment. Davis subsequently proposed that dopamine abnormalities occur in specific regions of the brain, which provided a rational explanation for the absence of abnormally elevated dopamine metabolites in cerebrospinal fluid and serum for schizophrenia (Davis, Kahn, Ko, & Davidson, 1991). Subsequently, several studies reported elevated dopamine synthesis in the presynaptic striatum in schizophrenia (Howes et al., 2009; McGowan, Lawrence, Sales, Quedsted, & Grasby, 2004; Meyer-Lindenberg et al., 2002). To determine the cause of

elevated dopamine synthesis, various radiotracers were utilized in imaging studies, and several studies reported elevated D2 and D3 receptors in striatal regions (Buchsbaum et al., 2006; Kestler, Walker, & Vega, 2001; Takahashi, Higuchi, & Suhara, 2006). As for D1 receptors, some studies suggested that prefrontal cortex dopaminergic transmission is mediated by D1, and abnormalities in D1 receptor in the prefrontal cortex cause cognitive deficits and some negative behavioral manifestations in schizophrenia (Abi-Dargham et al., 2022). Due to different radiotracers used, the decreasing and increasing of D1 receptors have been both reported in different studies (Karlsson, Farde, Halldin, & Sedvall, 2002; Okubo et al., 1997).

In addition to the dopamine receptor hypothesis, studies in recent years have shown that glutamatergic synaptic dysregulation is also associated with schizophrenia. Nowadays, antipsychotic drugs are now poorly tolerated. Some researchers have suggested that abnormal N-methyl-D-aspartic acid receptor (NMDA) receptor function may be the key to the symptoms of drug resistance (Coyle, 2006). Yurgelun-Todd et al. found a significant reduction in gamma-aminobutyric acid (GABA) levels in the prefrontal cortex of patients through autopsy of schizophrenia (Yurgelun-Todd et al., 2005). Besides, the reduced levels of GABA receptors may be due to NMDA receptor hypofunction (Woo, Walsh, & Benes, 2004). In healthy individuals, the use of NMDA receptor antagonists such as Phencyclidine-D5 Hydrochloride (PCP) and ketamine causes schizophrenia-like and persistent psychosis-negative cognitive symptoms for two weeks. In addition to this, Warren et al. found that approximately 6.5% of patients showed positive NMDA receptors at their first onset of illness (Warren, Siskind, & O'Gorman, 2018), providing direct evidence for the NMDA receptor hypothesis.

1.4.2.2 Brain Imaging

Structural Magnetic Resonance Imaging (SMRI) and Functional Magnetic Resonance Imaging (fMRI) provide evidence of structural and functional changes in the brain in schizophrenia. Their non-invasive properties allow them to track changes in the course of schizophrenia over time, which facilitates future diagnostic techniques for schizophrenia and the continuous updating of treatment guidelines.

From a structural perspective, researchers have identified abnormal changes in multiple brain regions in SCZ patients. Several studies have found gray matter atrophy as well as reduced white matter in the frontal lobe, temporal lobe, thalamus, and occipital

lobe in SCZ patients, and a prominent reduction in hippocampal subfield volume(Andreasen et al., 2011; Hu et al., 2020; Tesli et al., 2020). In addition to this, Delisi, Sharma and Shenton, et al. observed asymmetrical deviations in two cerebral hemispheres in SCZ patients, and these asymmetrical regions were present in the temporal, frontal, and occipital lobes(DeLisi et al., 1997; Sharma et al., 1999; Shenton, Dickey, Frumin, & McCarley, 2001). Jiang et al. found the progressive atrophy process of gray matter by tracing the gray matter of the brain at different course stages of the disease(Jiang et al., 2018).

For the causes of schizophrenia, brain disconnection is the more widely recognized hypothesis. Friston and Frith first proposed that the dysfunction of communication within the brain of schizophrenia is the main cause of the symptoms(Friston & Frith, 1995). Later on, researchers gave extensive supplements from the abnormalities of structural and functional brain connectivity of SCZ.

In terms of structural connectivity, Csernansky et al. found disruption of frontal-striatal-thalamic circuits in SCZ patients (Csernansky & Cronenwett, 2008). Price et al. found an abnormal distribution of anisotropy (FA) in the left uncinate fasciculus, a maximal white matter bundle connecting the frontal and temporal lobes, in the first episode of SCZ patients (Price et al., 2008). Andrew et al. constructed a structural network based on Diffusion Tensor Imaging (DTI) and analyzed the network properties of SCZ patients. They found that SCZ patients had impaired connectivity in a distributed lymph node network including the medial frontal, parietal, and left temporal lobes(Zalesky et al., 2011). Ellison-Wright et al. summarized current research on structural connectivity based on DTI and found that there is reduced white matter in the left frontal and left temporal lobes and the white matter bundle networks associated with these two regions may be affected(Ellison-Wright & Bullmore, 2009). In terms of functional brain connectivity in SCZ patients, Andrew et al. found that the dysfunctional connectivity of the sub-network mainly involves connectivity between the frontal and temporal lobe in the left hemisphere, and functional connectivity disruptions have also been demonstrated in the parietal lobe, occipital lobe, and other regions(Zalesky et al., 2010). Subsequent reports by Liu, Repovs, et al. have all verified dysfunction of frontal and temporal lobe functional connectivity and found that connectivity disruptions are also present in other brain regions, such as occipital, parietal, and cerebellar regions (Liu et al., 2008; Repovs, Csernansky, & Barch, 2011).

In conclusion, both anatomical and functional connectivity studies have revealed significant alterations in frontotemporal connectivity pathways, as well as significant alterations in the connectivity of brain regions such as the parietal and occipital lobes. This suggests that disruptions of brain connectivity may be prevalent in SCZ patients.

1.4.2.3 EEG in Schizophrenia

Although MRI boasts high spatial resolution and enables direct observation of neural substrates associated with schizophrenia during specific tasks, it fails to reveal rapid changes in brain activity within milliseconds. Therefore, EEG can provide a complementary perspective on the pathophysiological mechanisms

Shim achieved a classification accuracy of 78.24% by selecting features from the scalp and source EEG to classify healthy controls and SCZ patients (Shim, Hwang, Kim, Lee, & Im, 2016). Consistent with findings from MRI, the majority of discriminative features originated from the frontal and temporal lobes. Additionally, several studies have reported abnormalities in multiple rhythms in SCZ patients, such as increased activity in the delta and theta bands during resting states (Narayanan et al., 2014; Sponheim, Clementz, Iacono, & Beiser, 1994). Furthermore, SCZ patients exhibit impairments in facial emotion recognition and auditory processing. Jung et al. found reduced activities in the superior frontal gyrus and inferior frontal gyrus in SCZ patients, and there is a potential gender difference in facial emotion processing in SCZ patients (H.-T. Jung, Kim, Kim, Im, & Lee, 2012).

In numerous family risk studies of SCZ, the classical auditory oddball paradigm has been widely employed to investigate EEG abnormalities in SCZ. Many studies have reported reduced P3b amplitude in both SCZ patients and their first-degree relatives. This suggests that P300 may serve as a susceptibility marker for psychotic disorders (Kidogami, Yoneda, Asaba, & Sakai, 1991). Şevik et al. found a decrease in mismatch negativity (MMN) amplitude during working memory processes in both SCZ patients and their relatives (Şevik et al., 2011). This may indicate impaired working memory in both SCZ patients and their relatives. Narayanan, through ICA, also identified increased slow β activity in the frontal-central region and δ activity in the frontal lobe in individuals with SCZ patients and their relatives (Narayanan et al., 2014).

Furthermore, various functional brain network analysis methods have been employed in the analysis of abnormal brain activity in SCZ patients. Yeragani et al.

observed a significant reduction in coherence between the frontal and central regions in the β and γ frequency bands in early-onset SCZ patients (Yeragani, Cashmere, Miewald, Tancer, & Keshavan, 2006). Jalili utilized partial correlation to construct the EEG network and found significantly higher modularity in the β frequency band in SCZ patients compared to the healthy controls (Jalili & Knyazeva, 2011). Besides, the degrees of the frontal lobe, left occipital lobe, left temporal lobe, and right temporal lobe in SCZ patients are higher than those in the control group. Dynamic network analysis revealed decreased strength in the frontal, parietal, and sensorimotor areas during the Sustained Attention to Response Task (SART) stimulus process in SCZ patients (Naim-Feil et al., 2018). This was accompanied by a significant increase in global efficiency and a decrease in both global and local clustering coefficients.

In conclusion, EEG research unveils dynamic changes in brain activity in schizophrenia, providing an electrophysiological basis for understanding cognitive and functional impairments in schizophrenia. This knowledge contributes to the diagnosis and treatment of schizophrenia by offering electrophysiological insights. In this thesis, we will provide insights into abnormal network dynamics in SCZ patients from an electrophysiological perspective, based on CHD analysis, which complements the possible causes and diagnostic strategies for abnormal cognitive functioning in SCZ patients.

1.5 The Main Contributions of this Thesis

Due to the low signal-to-noise ratio (SNR) of EEG signals and the rich disease information embedded in EEG, this thesis explores the application of graph spectral theory to the analysis of EEG, and developing corresponding algorithms of EEG denoising and extraction of graph spectral features. The main contributions are as follows:

1. Noise can greatly affect the construction of subsequent analysis models for disease and cognition as well as the decoding efficiency of brain-computer interfaces. The graph filter developed from the graph spectral theory take into account the dependence between different channels of the brain, which is a promising denoising algorithm in the future. However, few algorithms consider denoising EEG using both temporal and underlying graph structure constraints. For this reason, we propose to solve the problem with a JFT filter based on the traditional graph spectral theory. To verify the robustness and effectiveness of the algorithm, we designed three sets of noise addition simulation

experiments and two sets of classification experiments with P300 real data. The results of the simulation experiments and classification experiments verify that the joint spatio-temporal framework can take into account both structural and temporal constraints on the EEG signal, and has stronger suppression of noise.

2. SCZ is associated with severe neurocognitive deficits and these neurocognitive deficits can be used as one of the diagnostic strategies for SCZ patients. Currently, the neural mechanisms of SCZ and the exploration of neurophysiological endophenotypes need to be further explored. The second project of the thesis focuses on feature extraction of graph spectral theory to explore the relationship between graph harmonics, cognitive abnormalities, and EEG rhythm in SCZ patients. The CHD method developed from graph spectral theory is a reliable tool for the analysis of brain network dynamics. Currently, few studies have explored the altered brain spatiotemporal network dynamics of SCZ patients as well as the rhythmic abnormalities of SCZ patients under the source space from a connectome harmonic perspective to find objective and reliable neurophysiological endophenotypes. Thus, this thesis utilizes CHD to explore EEG features of SCZ patients based on graph spectral theory. Specifically, we explored the changes of cognitive scales and ERPs of SCZ patients, which will support the reliability of our preprocessing and subsequent analyses. To explore the connectome harmonic abnormalities of SCZ patients and their connection with cognition, we first obtained the graph power spectral density (GPSD) of all harmonics and explored the relationship between neurocognitive abilities. Then, since different harmonics correspond to different spatial distributions of brain activities and support different EEG rhythms, to investigate the rhythmic changes of SCZ patients compared with healthy controls in different graph harmonics, the high-frequency and low-frequency graph filters are used to obtain the graph low-frequency signals (aligned signals) and high-frequency signals (liberal signals) and their activation patterns with Power Spectral Density (PSD). Finally, the captured differential features were used to predict the individual cognitive task scores. Our results reveal abnormal brain activity in SCZ patients and its relationship to cognitive performance and provide potential technical support for the diagnosis of SCZ patients. In addition, the relationship between harmonics and EEG rhythms and cognitive patterns also supports the reliability of the graph spectral theory for the application of dimensionality reduction and denoising.

1.6 Organization of the Thesis

This thesis develops corresponding EEG denoising and feature extraction algorithms based on graph spectral theory. The whole thesis consists of five chapters, and each chapter is organized as follows.

Chapter 1 Introduction, mainly introduces the theoretical knowledge related to this thesis from four aspects. The first part includes the application of EEG rhythm and EEG, as well as the application of graph spectral theory in brain science. Then we introduce the common noise in EEG and the current denoising techniques in EEG signals. Then we discuss the current research on schizophrenia and finally introduce the main work of this thesis and the structural arrangement of the thesis.

Chapter 2 JFT Filter for EEG Denoising Based on Graph Spectral Theory. First, the basic knowledge of graph spectral theory is introduced, followed by the introduction to the joint time-vertex framework and the corresponding denoising and classification algorithms. Then the data and simulation noises used in the thesis are presented followed by a detailed analysis and discussion of the results.

Chapter 3 Analysis of schizophrenia based on graph spectral theory. First, the data and the data processing flow are illustrated in this chapter, followed by an introduction to the specific techniques used such as the source localization algorithm, the graph spectral power density, the power spectral density, etc., and a detailed analysis and discussion of the results.

Chapter 4 General discussion. The key findings and significance and future research will be future discussed in this section. The limitations of this study and an outlook on future research will be presented in this chapter.

Chapter 2 JFT Filter for EEG Denoising Based on Graph Spectral Theory

2.1 Abstract

EEG has rich brain information and its acquisition is convenient and non-invasive. Thus, it is widely used in disease diagnosis, cognitive research, and brain-computer interfaces. However, EEG are susceptible to various noise interferences during the acquisition process, which affects the construction of computational cognitive models. Thus, the development of corresponding denoising algorithms is a necessary and challenging task. Previously, researchers have mainly addressed this problem through time-frequency algorithms and blind source analysis methods. However, the brain is an interactive system. To ensure normal cognitive function, all brain regions in the cortex work together and their information transmission is constrained by the underlying structural connectivity network. Traditional denoising algorithms do not take into account the mutual constraints between these brain regions, which may result in missing information. Graph spectral theory naturally represents EEG signals as graph signals and realizes noise removal through the relatively stable invariance of the connection distances between electrodes. It has been widely used as a reliable denoising technique in DTI, MRI, and EEG studies. In the thesis, considering the strong temporal resolution of EEG signals, the graph filter alone may not be sufficient to cope with complex noise conditions. So, we introduce a joint time-vertex framework into the EEG denoising based on the traditional graph spectral theory by applying graph domain-informed constraints and temporal smoothing constraints on the signals. A series of experimental results show that compared with the current traditional methods, the method proposed in this chapter has a strong suppression of different noises and can improve the decoding efficiency of the signals, which can be used in the preprocessing of EEG.

In application validation, as a kind of event-related potential P300 is one of the most studied and widely used components and is also widely used in the research of diseases and brain-computer interfaces. This thesis mainly explores the application of this denoising algorithm in P300 signals. It will provide a new idea for the future development of the denoising technology of EEG.

2.2 Introduction

When humans receive an external stimulus (e.g., a visual stimulus, etc.), the corresponding sensory cortex of the brain will recognize and interpret the stimulus. If the stimulus is recognized as requiring attention and memory, posterior regions of the brain, such as the parietal lobe, will generate the corresponding P300 signals. Sutton et al. recorded subjects' EEG responses to unidentified stimuli and they found a brain wave associated with the appearance of a target stimulus for the first time (Sutton, Braren, Zubin, & John, 1965). This positive waveform appeared as positive waveform approximately 300ms after the stimulus, hence it was named P300.

More studies have since found that P300 is associated with cognitive processing and attention, and is therefore widely used in neuroscience research and brain-computer interfaces. For example, a significant decrease in the P300 amplitude can be observed in patients with psychiatric disorders such as schizophrenia (Kidogami et al., 1991) and bi-directional affective disorder (Wada et al., 2019). Thus, P300 is often used in diagnostic studies of such psychiatric disorders. In addition to this, P300 does not depend on the training and can be produced by almost everyone's brain after receiving the target stimulus. As a result, researchers have proposed a series of brain-computer interface paradigms. Polikoff et al. proposed a brain-computer interface paradigm to use P300 signals in controlling the movement of the computer screen cursor (Polikoff, Bunnell, & Borkowski Jr, 1995). Then Farwell et al. first proposed a system for spelling based on P300 (Farwell & Donchin, 1988). Donchin et al. improved the system (Donchin, Spencer, & Wijesinghe, 2000), by replacing the original commands such as space and quit with the numbers, resulting in the system interface that is now commonly used in the P300 spelling system, as shown in Figure 2.1 below. The system provides the user with a 6×6 matrix and each cell contains an alphabet. The user is required to focus on the cell containing the letter to be texted. The rows and columns of the matrix are randomly highlighted. Therefore, only those highlighting events that contain the text of the spelled character will elicit P300. This is the same system used for Data 2 in this thesis.



Figure 2.1 P300 Spelling System Interface

However, one of the main problems in analyzing event-related potential (ERP) such as P300 is that the amplitude of the single-trial response is small compared to background EEG. Besides, the ERP is also susceptible to contamination by the noise generated by the acquisition system and other noise such as electromyographic artifacts during acquisition. Trial averaging (Da Silva & Wilkins, 1999), the most commonly used technique, assumes that the ERP signal occurs at relatively stable time points and enhances the signal-to-noise ratio of the ERP by averaging all trials. However, the repetitive time is long for some experiments, which creates a serious burden for both subjects and collectors. To obtain a stable ERP within a small number of trials, various modern signal processing techniques such as independent component analysis (T.-P. Jung et al., 1997), Bayesian averaging (Sparacino, Milani, Arslan, & Cobelli, 2002), principal component analysis (Chapman & McCrary, 1995), wavelet transform (Carmona & Hudgins, 1994), and deep learning (Zhang et al., 2021) are used in EEG signal processing.

In fact, the brain is a complex network system. We can consider brain signals as graph signals, and these information processing units as nodes in the graph. However, none of the above methods we mentioned has been able to fully utilize the potential intra- and inter-channel dependencies of EEG signals. To address this limitation, graph-based methods have received increasing attention in the field of biomedical signal processing. Graph signal processing techniques developed from graph spectral theory can utilize the underlying structure of the data and process signals on irregular grids. Complex problems

such as denoising of graph signals or signal diffusion can be solved by appropriate algorithms of graph spectral theory (Pentari et al., 2021, 2022). Compared with previous algorithms, this thesis focuses on the ability of spatiotemporal constraints under the l_{pq} -norm for denoising EEG based on graph spectral theory and explores the application of this algorithm in ERP processing such as P300. The composite constraint framework will also present some new ideas and insights for the development of subsequent denoising algorithms.

2.3 JFT Graph Filter

In this subsection, we will focus on the basics of graph spectral theory, the joint time-vertex framework, and the l_{pq} -norm JFT graph filter.

2.3.1 The Basics of Graph Spectral Theory

For social, energy, and neuronal networks, these high-dimensional data naturally reside on weighted graph vertices. The emerging field of Graph Signal Processing (GSP), which developed from graph spectral theory, combines algebraic and spectral graph theoretical concepts with computational harmonics to process graph signals and develops concepts that correspond to Digital Signal Processing (DSP) (R. Li et al., 2021; Ortega, Frossard, Kovačević, Moura, & Vandergheynst, 2018; Shuman, Narang, Frossard, Ortega, & Vandergheynst, 2013), such as filtering, shift, and modulation.

Assuming that the single-channel signal of the EEG is $s_n, n = 0, 1, \dots, N-1$, where N is the number of sample points, the polynomial representation of the z-transform of s_n is shown in Eq. (2-1). The unit time shift of the DSP can be obtained as shown in Eq. (2-2). Similarly, the FIR filter can be expressed in polynomial form as shown in Eq. (2-3).

$$s(z) = \sum_{n=0}^{N-1} s_n z^{-n} \quad (2-1)$$

$$s_{out} = h_{shift} \cdot s_{in} = (s_{N-1}, s_0, s_1, \dots, s_{N-2}), h_{shift} = z^{-1} \quad (2-2)$$

$$h(z) = \sum_{n=0}^{N-1} h_n z^{-n} \quad (2-3)$$

One of the important concepts to establish a link between GSP and DSP is the shift-invariance of DSP. In DSP, we can easily obtain the mathematical expression for the shift-invariance of DSP as shown in the following equation:

$$z^{-1}h(z) = h(z)z^{-1} \quad (2-4)$$

In graph signal processing, its sample points are no longer time points, the nodes of the graph. The EEG signal at time t is $s = [s_0 s_1 \dots s_{N-1}]^T \in C^N$, where N is the number of EEG electrodes. Similar to the unit time shift of a DSP, the unit shift of the graph signal can be obtained by a unit cyclic matrix A_c as shown in Eq. (2-5).

$$[s_{N-1} s_0 s_1 \dots s_{N-2}]^T = A_c \cdot [s_0 s_1 \dots s_{N-1}]^T \quad (2-5)$$

$$A_c = \begin{bmatrix} 0 & 0 & 0 & \dots & 0 & 1 \\ 1 & 0 & 0 & \dots & 0 & 0 \\ 0 & 1 & 0 & \dots & 0 & 0 \\ \vdots & \vdots & \ddots & \ddots & \ddots & \vdots \\ 0 & 0 & \dots & 1 & 0 & 0 \\ 0 & 0 & \dots & 0 & 1 & 0 \end{bmatrix} \quad (2-6)$$

The graph filter H or graph signal H can be represented by the polynomial form of A as shown in Eq. (2-7). $A = V\Lambda V^{-1}$ can be represented by its eigenvectors, where $V = [v_1, \dots, v_m, \dots, v_n]$. That the $h(\lambda_m)$ is the characteristic function of the polynomial filter H as shown in Eq. (2-8). The exponential function $h(\lambda_m)$ is a characteristic function of a linear system, which means that when the input signal is exponential, the response of the system is also exponential. This concept corresponds to the exponential invariance of DSP.

$$\begin{aligned} H &= h(A) \\ &= h(V\Lambda V^{-1}) \\ &= \sum_{m=0}^{M-1} h_m(V\Lambda V^{-1})^m \\ &= Vh(\Lambda)V^{-1} \end{aligned} \quad (2-7)$$

$$\begin{aligned} Hv_m &= Vh(\Lambda)V^{-1}v_m \\ &= Vh(\Lambda)e_m \\ &= h(\lambda_m)v_m \end{aligned} \quad (2-8)$$

Similarly, we can obtain the mathematical representation of the Graph Fourier Transform (GFT) as shown in Eq. (2-9), and the mathematical representation of its inverse transform as shown in Eq.(2-10).

$$\hat{s} = Fs = V^{-1}s = [f_0 s \dots f_{N-1} s]^T \quad (2-9)$$

$$s = F^{-1}\hat{s} = V\hat{s} = \sum_{k=0}^{N-1} \hat{s}_k v_k \quad (2-10)$$

So far, basic concepts like graph filtering and graph Fourier transform in graph signal processing are introduced in the subsection. Similar to the wavelet transform, there are several choices of cyclic matrices A for the graph transform, and the most common one is the Laplacian matrix $L = D - A$ rather than the unit cyclic matrix A_c . In fact, the Laplacian matrix is the Laplacian operator on the graph, which responds to the integral of the gains generated when a single node is perturbed with respect to other nodes. Moreover, the graph Laplacian matrix is a symmetric semi-positive definite matrix and its zero eigenvalue is equal to the number of connected components of the graph. This property has also led to the graph Laplacian operator being commonly used in classification. On the other hand, the eigenvectors of the Laplacian matrix have spectral properties that are associated with the structural and topological properties of the graph. Usually, smaller eigenvalues and their corresponding eigenvectors correspond to the global structure of the graph, and larger eigenvalues and their corresponding eigenvectors correspond to the local structure of the graph. This makes the Laplace matrix the most commonly used matrix for constructing graph harmonics in graph signal processing.

2.3.2 Joint Time-vertex Framework

We assume that the EEG signal is $X = [x_1, x_2, \dots, x_T] \in R^{N \times T}$. $G = (V, \mathcal{E}, W)$ is the undirected graph in which the EEG signal resides, where V is the EEG acquisition channel (node in graph), \mathcal{E} is the set of functional or structural connectivity edges, $W \in R^{N \times N}$ is the symmetric weight matrix. W can be estimated by the physical or functional connectivity distances between leads. The matrix W in this thesis can be estimated by the following Eq.(2-11), where $x_i \in R^{1 \times T}$ is the signal of the i th channel. In W , the distance weights of the first k nearest leads to each lead are ultimately retained.

$$W_{ij} = e^{-\frac{\|x_i - x_j\|^2}{t}} \quad (2-11)$$

The Discrete Fourier Transform (DFT) provides a means of decomposing a signal into a series of harmonic modes. For example, the DFT for an EEG signal can be obtained from the following equation.

$$DFT\{X\} = X\bar{U}_T \quad (2-12)$$

$$U_T^*(t, k) = \frac{e^{-jw_k t}}{\sqrt{T}}, w_k = \frac{2\pi(k-1)}{T} \quad (2-13)$$

Similarly, EEG as a graph signal can be decomposed into a series of graph harmonics. The Graph Fourier Transform (GFT) of the signal can be obtained with Eq.(2-14) below. In graph signal processing, the graph harmonics refer to the eigenvectors of the Laplacian matrix, which can be obtained by equations(2-15) and (2-16).

$$GFT\{X\} = U_G^* X \quad (2-14)$$

$$L_G = I - D^{-\frac{1}{2}} W D^{-\frac{1}{2}} \quad (2-15)$$

$$L_G = U_G \Lambda_G U_G^* \quad (2-16)$$

Finally, we can decompose the signal X into harmonic oscillations in time and space. Then the Joint time-vertex Fourier transform (JFT) of the signal can be given as follows:

$$JFT\{X\} = U_G^* X \bar{U} \quad (2-17)$$

where its vector expression is given by the following equation

$$JFT\{x\} = U_J^* x, U_J = U_T \otimes U_G \quad (2-18)$$

2.3.3 Graph Smoothing Filter Based on the l_{pq} norm

Before introducing graph filters, what we need to understand is the variation in time and graph. Let the one-dimensional differential operator of X in time be ∇_T^T , where $X \nabla_T^T|_t = x_t - x_{t-1}$. Then the time Laplacian matrix $L_T = \nabla_T^* \nabla_T$ is the discrete-time second-order derivative operator, where $X L_T|_t = -x_{t+1} + 2x_t - x_{t-1}$. The singular value decomposition of L_T is as follows:

$$L_T = U_T \Lambda_T U_T^*, \Lambda_T(k, k) = 2(1 - \cos(w_k)) \quad (2-19)$$

Similarly, the derivative of the graph signal X with respect to the edge $e = (n, m)$ at node n on the graph is obtained as:

$$\frac{\partial X}{\partial e}|_n = \sqrt{W(n, m)} [x_n - x_m] \quad (2-20)$$

Then the graph divergence of the graph signal X at node n is

$$\nabla_G x|_n = \left\{ \frac{\partial X}{\partial e} \Big|_{e \in \mathcal{E}} \right\} \quad (2-21)$$

Similarly, $L_G = \nabla_G^* \nabla_G$ as a second-order gradient operator on the graph can be obtained. The two gradient operators are merged to obtain the joint gradient operator ∇_J of signal X in graph and time.

$$\nabla_J = \begin{bmatrix} \nabla_T \otimes I_G \\ I_T \otimes \nabla_G \end{bmatrix} \quad (2-22)$$

At this point, the total smoothness of the signal X in time and space can be measured by the gradient ∇_J , as shown in Eq. (2-23)

$$\|\nabla_J x\|_2^2 = x^T L_J x = \|\nabla_G X\|_F^2 + \|X \nabla_T\|_F^2 \quad (2-23)$$

where $\|\nabla_G X\|$ and $\|X \nabla_T\|$ represent the smoothness or continuity of the signal in space and time, respectively.

Next, the l_{pq} norm of the temporal and spatial smoothing of signal X can be used to solve the artifact-free signal X from the noisy signal by solving the optimal solution of (2-24).

$$\arg \min_X \|X - Y\|_F^2 + \alpha \|X \nabla_T\|_p^p + \beta \|\nabla_G X\|_q^q \quad (2-24)$$

The following part will discuss how to obtain the optimal solution of Eq. (2-24) in different cases. When $p = 2$ and $q = 2$, we need to obtain the optimal solution of Eq.(2-25).

$$\begin{aligned} & \arg \min_X \|X - Y\|_F^2 + \alpha \|X \nabla_T\|_F^2 + \beta \|\nabla_G X\|_F^2 \\ & = \arg \min_X \|X - Y\|_F^2 + \alpha \text{tr}(X L_T X^T) + \beta \text{tr}(X^T L_G X) \end{aligned} \quad (2-25)$$

Assuming $h(X) = \|X - Y\|_F^2$, $g(X) = \|\nabla_G X\|_F^2$, $h(X)$ and $g(X)$ are differentiable. Therefore, the optimal solution of Eq. (2-25) can be obtained by the following equation (2-26).

$$\begin{aligned} L(X) &= \|X - Y\|_F^2 + \alpha \text{tr}(X L_T X^T) + \beta \text{tr}(X^T L_G X) \\ L'(X) &= 2(X - Y) + \alpha(L_T + L_T^T)X + \beta(L_G + L_G^T)X \\ &= 2(X - Y) + \alpha 2L_T X + \beta 2L_G X = 0 \\ X &= (I + \alpha L_T + \beta L_G)^{-1} Y \\ X &= HY, h(\lambda_l, w_k) = \frac{1}{1 + 2\alpha(1 - \cos(2\pi w_k)) + \beta \lambda_l} \end{aligned} \quad (2-26)$$

where H is the final derived graph filter.

When $p = 2, q = 1$, since $h(X) = \|\nabla_G X\|_1$ is not differentiable, X can be solved by the FISTA algorithm. Assuming $f(X) = \|X - Y\|_F^2 + \alpha \|X \nabla_T\|_F^2$, Eq.(2-24) can be divided into the following two equations

$$\arg \min_{u_2} \|u_2 - Y\|_F^2 + \alpha \|u_2 \nabla_T\|_F^2 \quad (2-27)$$

$$\text{prox}_{\gamma h}(u_2) = \arg \min_X \frac{1}{2} \|X - u_2\|^2 + \frac{\beta}{\gamma} \|\nabla_G X\|_1 \quad (2-28)$$

Table 2.1 FISTA algorithm

FISTA algorithm
Input: Contaminated signal Y, α, β
Set $u_1 = Y, t_1 = 1, \gamma = 1$,
While not converged do:
$u_2 = u_1 - \gamma(2(u_1 - Y) + 2L\alpha u_1)$
$X_k = \text{prox}_{\gamma h}(u_2)$
$t_2 = (1 + \sqrt{1 + 4t_1^2}) / 2$
$u_1 = X_k + (t_1 - 1)(X_k - u_1) / t_2$
$u_1 = X_k$
$t_1 = t_2$
end

Then, the signal X can be derived by the FISTA algorithm shown in Table 2.1, where $L = L_G$ and $\text{prox}_{\gamma h}(u_2)$ is as shown in (2-28). Similarly, when $p = 1, q = 2$, the FISTA algorithm is still needed to solve X. At this time, some of the parameters in the iteration are shown as follows:

$$L = L_D \quad (2-29)$$

$$\text{prox}_{\gamma h}(u_2) = \arg \min_X \frac{1}{2} \|X - u_2\|^2 + \frac{\alpha}{\gamma} \|\nabla_T X\|_1 \quad (2-30)$$

$$u_2 = u_1 - \gamma(2(u_1 - Y) + 2L\beta u_1) \quad (2-31)$$

In this thesis, the solution of Eq. (2-28) and Eq. (2-30) refer to the direct solution algorithm based on the total time variation of the l_1 -norm proposed by Condat(Condat, 2013) and the algorithm proposed by Fadili(Fadili & Starck, 2009), respectively.

When $p = 1, q = 1$, since both $h(X) = \alpha \|X \nabla_T\|_1$ and $g(X) = \beta \|\nabla_G X\|_1$ are not differentiable, Forward-Backward-Based Primal-Dual algorithm is used to obtain

artifact-free signal X . The flow of the algorithm is shown in Table 2.2, where $prox_{\gamma h}$ and $prox_{\sigma g^*}$ are shown in equations(2-30) and (2-32) respectively.

$$prox_{\sigma g^*}(x) = \arg \min_z \frac{1}{2} \|x - z\|_F^2 + \frac{1}{\sigma} g^*(z) \quad (2-32)$$

Table 2.2 FB-based primal-dual algorithm

FB-based primal-dual algorithm for JFT11
Input: Contaminated signal Y , α , β
Set $x_0 = Y, \tau = 1/2, \sigma = 1$
While not converged do:
$g = 2(x_n - Y)$
$p_n = prox_{\tau h}(x_n - \tau(g + L_T v_n))$
$q_n = prox_{\sigma g^*}(v_n - \sigma L_G(2p_n - x_n))$
$x_{n+1} = x_n + \lambda(p_n - x_n)$
$v_{n+1} = v_n + \lambda(q_n - v_n)$
end

We can find the solution to Eq. (2-32) as shown in Eq. (2-35) with the More decomposition property of the proximal operator shown in Eq.(2-33), where $prox_h(x)$ is shown in Eq.(2-34).

$$x = prox_h(x) + prox_{h^*}(x) \quad (2-33)$$

$$prox_h(x) = \arg \min_u h(x) + \frac{1}{2} \|u - x\|_2^2 \quad (2-34)$$

$$prox_{\sigma g^*}(x) = x - \frac{\beta}{\sigma} u \quad (2-35)$$

$$u = \arg \min_z \left\| \frac{\sigma x}{\beta} - z \right\|_F^2 + \frac{\sigma}{\beta} \|\nabla_G z\|_1 \quad (2-36)$$

2.3.4 Stepwise Linear Discriminant Analysis

The determination of the presence of evoked potentials P300 by EEG features is a binary problem with the decision hyperplane shown below:

$$w \cdot x - b = 0 \quad (2-37)$$

where w is a vector of feature weights, b is a bias term, and x is a feature vector.

Stepwise linear Discriminant Analysis (SWLDA) is a feature selection technique. It adds the most statistically significant predictor variable ($p < k$) to the model through a

combination of forward and backward stepwise regression, starting with no initial model term. After the model is updated, backward stepwise regression is performed to remove the least significant variables ($p > \varepsilon$). The process is then repeated until the model contains a predetermined number of variables or no other variables meet the input or removal criteria.

2.4 Simulation and Real Data Classification Results

We verify the robustness of the algorithm in simulation experiments and classification experiments on two P300 datasets, respectively. In this section, the experimental dataset, simulation noise, simulation results, and its classification results will be presented.

2.4.1 Dataset

Data I contained healthy and auditory hallucinated subjects. All participants signed informed consent forms (23 hallucinated subjects and 29 healthy subjects). To elicit event-related potentials, the auditory P300 oddball paradigm was applied to the data acquisition. In this study, we used Stmtop amplifier and 16-channel electrode caps to record P300 and resting-state EEG from both groups of subjects with a sampling rate of 1000 Hz, and all electrode impedances were kept below 5 K Ω .

To further validate the algorithm's effectiveness, we introduced dataset II (Wolpaw, McFarland, Vaughan, & Schalk, 2003), which is a publicly available P300 brain-computer interface dataset. For each character, the user display was as follows: the matrix was displayed for a 2.5 s period, and during this time, each character had the same intensity (i.e., the matrix was blank). Subsequently, each row and column in the matrix was randomly intensified for 100ms (i.e., resulting in 12 different stimuli – 6 rows and 6 columns). (After the intensification of a row/column, the matrix was blank for 75ms.). In this experiment, the signal was sampled at a rate of 240 Hz. Three participants are involved, with 2 in the training set with 11 sessions and 41 trials and 1 in the test set with 8 sessions. Each trial corresponds to one character.

2.4.2 Simulation Noise and Simulation Results

2.4.2.1 Simulation Noise

To verify the validity of the algorithm, dataset I was rigorously preprocessed to obtain ground-truth ERP signals in this thesis. The EEG of healthy subjects was first filtered through a low-pass filter of 1-20 Hz. Then electromyographic artifacts were removed by ICA. Finally, all the trials were averaged to obtain the robust P300. As a result, the averaged P300 signal is the ground truth. To verify the robustness of the algorithm to different noises, three types of noises were added to the baseline EEG signal, which are Gaussian noise, impulse noise, and spontaneous EEG noise.

Mathematically, Gaussian noise obeys a probability distribution with mean zero and standard deviation σ . The mathematical expression of its probability distribution is shown in the following Eq.(2-38). EEG is usually affected by a variety of noises, including physiological noise, environmental noise, and noise of the instrument itself. Some of the noises have similar distributions and properties to Gaussian noise, and thus Gaussian noise is often used in simulation.

$$f(x) = \frac{1}{\sqrt{2\pi}\sigma} e^{-\frac{(x-\mu)^2}{2\sigma^2}} \quad (2-38)$$

Here, the noise is considered as additive noise. As shown in Eq.(2-39), the contaminated noise Y is modulated by the original EEG X_{ori} and the noise S . The intensity of noise was controlled by the signal-to-noise ratio as shown in Eq. (2-40).

$$Y = X_{ori} + S \quad (2-39)$$

$$SNR = 10 \log_{10} \frac{\|X_{ori}\|_2^2}{\|S\|_2^2} \quad (2-40)$$

In addition to Gaussian noise, there is also a lot of non-Gaussian noise and impulse noise in the actual acquisition process. Here, the Alpha-stable distribution was used to model the impulse noise. The mathematical expression of Alpha-stable probability distribution is shown in Eq. (2-41). α is the characteristic index, which usually varies in $(0, 2]$ and mainly controls the thickness of the tail in the probability density function. The smaller its value is, the thicker the tail is. δ is the position parameter, which is set to 0 in

this experiment for the sake of generality. γ is the scale parameter, which describes the degree of deviation of the stable distribution from its mean value.

$$\Phi(t) = e^{(i\delta t - \gamma^\alpha |t|^\alpha)} \quad (2-41)$$

When $\alpha = 1.3, \delta = 0, \gamma = 1$, the pulse noise S is shown in Figure 2.2.

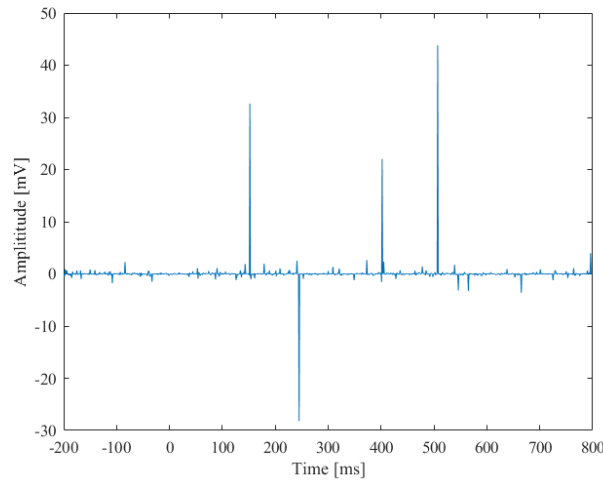


Figure 2.2 The impulsive noise

Finally, since the P300 is usually submerged in the resting-state EEG. In this thesis, the resting-state EEG of the subjects is used as one of the noise signals in the simulation. We will randomly cut out a segment from a 5-minute resting-state EEG and add it to the original EEG signal X_{ori} .

Finally, after denoising, the signal-to-noise ratio of the noise-reduced signal can be calculated through Eq.(2-42), where X_{de} is the signal after denoising.

$$SNR = 10 \log_{10} \frac{\|X_{ori}\|_2^2}{\|X_{de} - X_{ori}\|_2^2} \quad (2-42)$$

2.4.2.2 Simulation results

Before describing the results, Table 2.3 gives the description of the algorithm and the parameter settings for this thesis. Specifically, we compare 4-layer db5 wavelets commonly used for EEG denoising. Two soft thresholding methods are used for wavelet threshold estimation. They are rigrsure and sqtwolog, respectively. It is worth noting that DFTp means that the l_p -norm of temporal smoothing is used for denoising without spatial smoothing. JFTpq means that the l_p -norm of temporal smoothing and the l_q -

norm of graph smoothing are used as constraints. All simulation experiments were repeated 100 times and the average results of these 100 times were calculated.

Table 2.3 Description of algorithms and parameters

WT1	WT2	DFT _p	GFT _q	JFT _{pq}
db5	db5	p=2 or 1	p=0	p=1 or 2
rigrsure	sqtwolog	q=0	q=1 or 2	q=1 or 2
4 levels	4 levels			

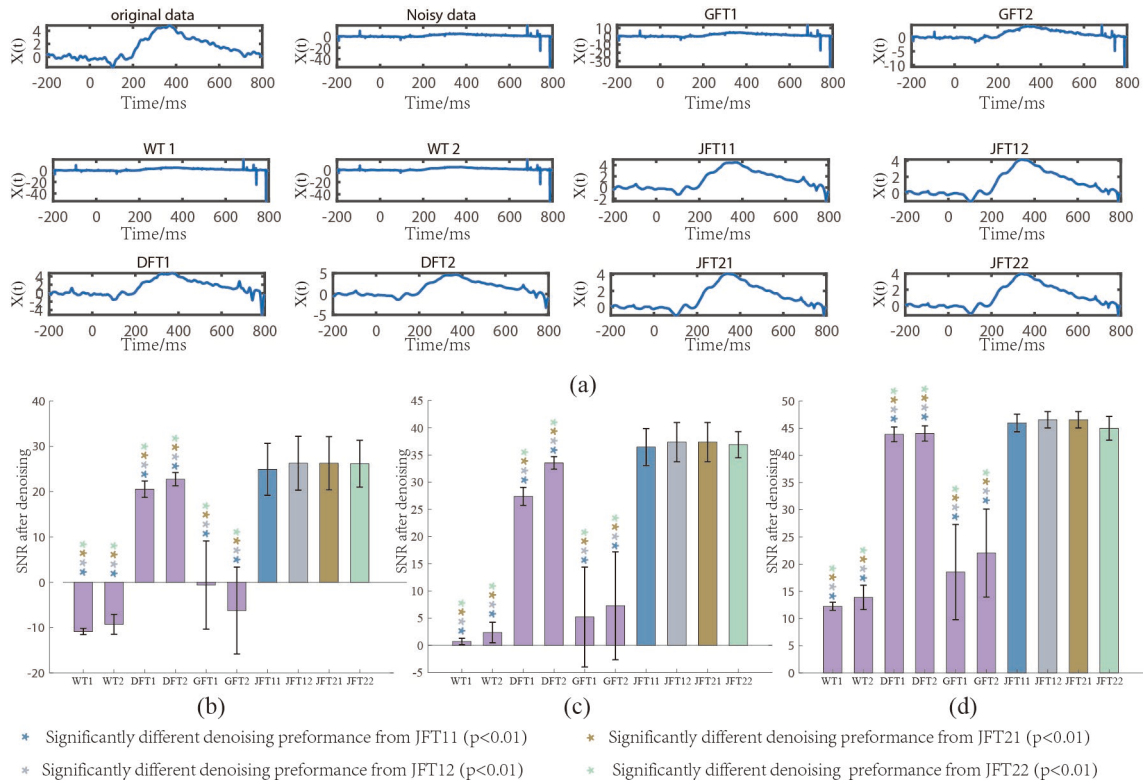


Figure 2.3 Schematic of the EEG waveforms and the SNR after denoising at different impulsive noise intensities: (a) EEG waveforms before and after denoising at SNR=0dB; (b) impulsive noise intensities SNR=-5dB; (c) impulsive noise intensities SNR=0dB; (d) impulsive noise intensities SNR=5dB

First, we added impulse noise to the C3 lead, after which we used algorithms to filter the EEG signal. Figure 2.3 shows the ERP waveforms after denoising with these 10 algorithms as well as the SNR after denoising under the contamination of different intensities of impulsive noise. Table 2.4 shows the quantitative results of the denoising ability of different algorithms under the contamination of different distributions of impulsive noise. Through the ERP waveforms shown in Figure 2.3 (a), we can observe

that the impulse noise amplitude is still as high as about 30-40 uV by the GFT1 and WT, whereas the impulse noise is suppressed by the GFT2. The impulse noise amplitude is weakened to less than 4 uV by the DFT2. JFT algorithm achieves even better impulse noise suppression and the impulse noise amplitude is almost minimized to 0. As shown in Figure 2.3(b) and (c), at noise intensities of -5dB and 0dB, the SNR of JFT after denoising is further significantly improved by 4dB compared to DFT2 ($p < 0.01$); while at noise intensity of 5dB, the SNR of JFT is still significantly improved by 2dB compared to DFT2 ($p < 0.01$). As shown in Table 2.4, we can see that no matter how the distribution parameters of the impulse noise, the SNR of WT1 and WT2 is still around -10dB, and GFT2 and GFT1 improve the SNR compared to WT. Meanwhile, the SNR of the DFT1 and DFT2 is basically at 20 dB and 22 dB. The JFT algorithm incorporates graph and temporal smoothing and further significantly improves the SNR ($p < 0.01$). The SNR of JFT is basically at about 26 dB after denoising. Overall, the JFT algorithm provides significantly better suppression of impulse noise compared to other algorithms.

Table 2.4 SNR (dB) after denoising at noise intensity of -5dB and different parameter distributions of impulse noise. ***: represents the algorithm has a significantly different denoising performance from JFT11, JFT12, JFT21, and JFT22, respectively

	$\alpha=1.1,$ $\gamma=1.5$	$\alpha=1.3,\gamma=$ 1.5	$\alpha=1.7,$ $\gamma=1.5$	$\alpha=2.0,$ $\gamma=1.5$	$\alpha=1.1,$ $\gamma=4.5$	$\alpha=1.3,$ $\gamma=4.5$	$\alpha=1.7,$ $\gamma=4.5$	$\alpha=2.0,$ $\gamma=4.5$
WT1***	-10.74	-10.84	-10.87	-10.86	-10.77	-10.87	-10.84	-10.78
WT2***	-8.94	-9.29	-9.36	-9.32	-9.09	-9.34	-9.30	-9.06
DFT2***	22.82	22.53	22.53	22.92	22.89	22.62	22.73	22.62
DFT1***	20.67	20.34	20.35	20.67	20.68	20.42	20.54	20.41
GFT2***	-2.08	-1.03	-1.48	-1.04	-2.85	-3.15	0.90	-2.30
GFT1***	-2.34	-0.91	-1.50	-0.75	-2.72	-3.15	0.59	-2.52
JFT11	27.29	27.43	27.24	27.64	26.99	26.66	28.22	26.93
JFT12	27.25	27.45	27.37	27.64	27.11	26.57	28.40	27.06
JFT21	27.19	27.45	27.37	27.64	27.11	26.57	28.40	27.06
JFT22	25.99	26.21	26.16	26.36	26.04	25.55	26.86	26.03

Figure 2.4 illustrates the ERP signal and the SNR after denoising under the contamination of different intensities of Gaussian noise. It is worth noting that, as shown in Figure 2.4(b), at noise intensities of -5dB, when only spatial smoothing is utilized, SNR with GFT is almost the same as or even worsens; while at noise intensities of 5dB, the GFT improves the SNR as shown in Figure 2.4 (d). In addition, compared with the wavelet transform, the SNRs of JFT22, JFT21, JFT11, and JFT12 are significantly higher than those of WT1 and WT2 ($p < 0.01$). Regardless of the changes in the Gaussian noise

intensity, the SNR of JFT11 and JFT21 are significantly improved by about 2 dB compared with the DFT2 ($p < 0.01$). In addition, from Figure 2.4 (a), we can observe that the signal tends to change more linearly in a short time when the DFT1 selects improper parameters.

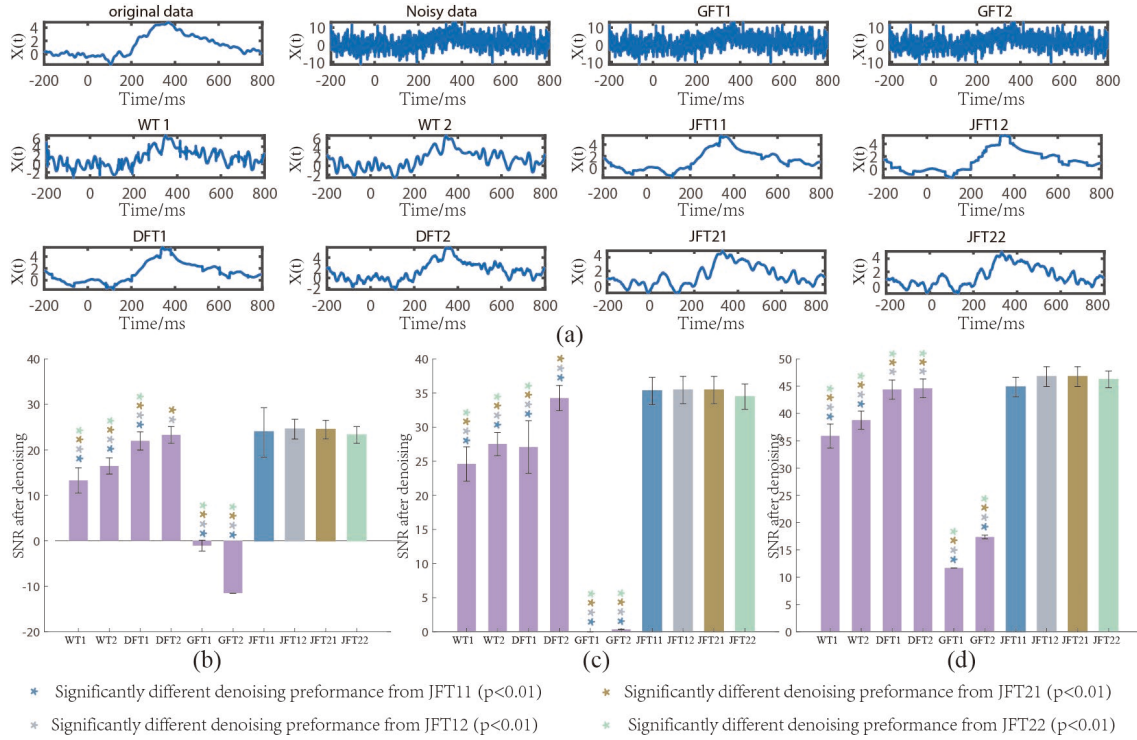


Figure 2.4 Schematic of the EEG waveforms and the SNR after denoising at different Gaussian noise intensities: (a) EEG waveforms before and after denoising at SNR=-5dB; (b) Gaussian noise intensities SNR=-5dB; (c) Gaussian noise intensities SNR=0dB; (d) Gaussian noise intensities SNR=5dB

Due to the low SNR of the P300 signal and the fact that P300 is usually submerged by resting EEG, resting EEG is regarded as a noise signal and its intensity is modulated by SNR. The denoising results are shown in Figure 2.5. We can observe from Figure 2.5 (a) is that the GFT algorithm extracts the main waveform of the signal, making the filtered P300 waveform more significant. In addition, we can notice that at noise intensities of -5dB, as shown in Figure 2.5(b), all the filtering algorithms are unable to improve the SNR. In Figure 2.5(c) and Figure 2.5(d), we can observe that compared to DFT, GFT has better suppression of spontaneous EEG noise, which significantly improves the SNR ($p < 0.01$). WT hardly improves the signal quality when SNR=0. The two algorithms, JFT12 and JFT21, further improved SNR compared to GFT ($p < 0.01$).

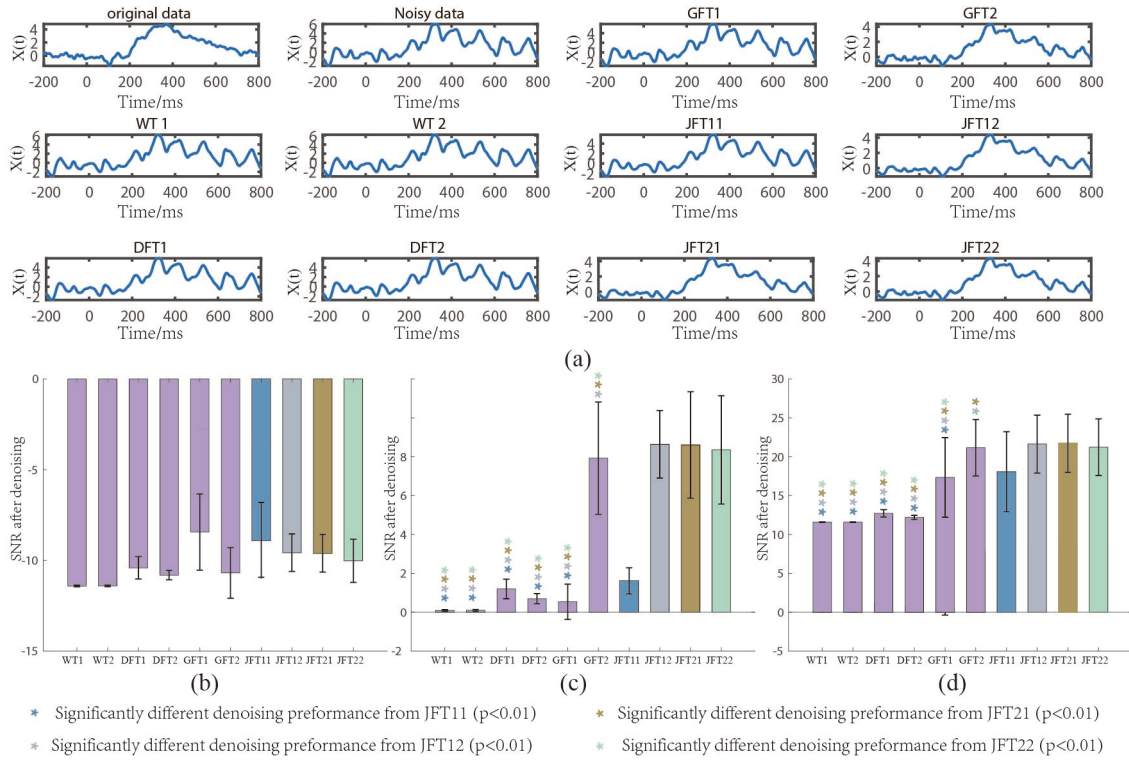


Figure 2.5 Schematic of the EEG waveforms and the SNR after denoising at different spontaneous noise intensities: (a) EEG waveforms before and after denoising at SNR=5dB; (b) spontaneous noise intensities SNR=-5dB; (c) spontaneous noise intensities SNR=0dB; (d) spontaneous noise intensities SNR=5dB

2.4.3 Classification Results

In order to further verify the effectiveness of the algorithm, the classification is further performed in real data. The signal is first filtered with different denoising algorithms, and then we construct the classification model using SWLDA.

Through the pre-simulation experiments, we can observe that both JFT21 and JFT22 show good noise suppression ability in the simulation experiments, whereas when using DFT1, improperly imposed parameter can lead to linear distortion of the signal. Therefore, in dataset 1, we mainly compare the two algorithms, JFT21 and JFT22, as well as DFT2, GFT, and WT algorithms. Dataset 1 mainly contains healthy subjects and auditory hallucinated patients with schizophrenia. The leave-one-out method was used for dataset segmentation. As shown in Table 2.5, the classification accuracy after JFT21 filtering reaches 82.69%.

Table 2.5 Classification accuracy in healthy controls and auditory verbal hallucinations from ERP(%)

Methods	Original data	DFT2	GFT2	WT1	WT2	JFT22	JFT21
Leave-1-out	69.23	73.08	71.15	71.15	69.23	78.85	82.69

In the P300 spelling system, our main goal is the Information Transfer Rate (ITR). Therefore, the signal classification accuracy should be increased while keeping the response time as short as possible. Due to the long iteration time of the l_1 -norm, we only check the effectiveness of the algorithms DFT2, GFT2, JFT22, and WT in dataset 2. The results of character spelling accuracy for signals filtered by different algorithms are shown in Table 2.6 below for the first 5 repetitive trials. We can find that after JFT22 is used for preprocessing, the character recognition accuracy of the P300 speller is significantly improved, and all characters can be recognized and decoded when the number of repetitions is 5.

Table 2.6 Character spelling accuracy with different denoising algorithms(%)

Methods	Repetitive trials				
	1	2	3	4	5
Original data	38.71	54.84	67.74	77.42	83.87
WT1	29.03	54.84	77.42	80.65	96.77
WT2	54.85	58.06	77.42	87.10	93.55
GFT	22.58	48.39	54.84	77.42	87.10
DFT	35.48	54.84	80.65	90.32	100
JFT22	58.06	67.74	83.87	96.77	100

2.5 Discussion

EEG signals are highly susceptible to noise during the acquisition process, and this inherent problem hinders the subsequent analysis of EEG, thus affecting the performance of brain-computer interfaces and clinical diagnostic models. In this thesis, we mainly explore the denoising performance of wavelet transform and JFT filters based on graph-temporal smoothing.

The experimental results show that, as shown in Table 2.4 and Figure 2.3, for impulse noise, WT has almost less suppression effect on impulse noise at low SNR conditions (SNR=-5dB). In contrast, DFT has a good suppression ability for impulse noise. Under a strong noise environment, GFT1 and GFT2 have weaker suppression ability on impulsive noises. JFT combines the advantages of GFT and DFT to further improve the signal quality of the noisy signal, which also suggests that GFT can further take effect after DFT

smoothing. Overall, the effectiveness of JFT on impulse noise suppression is better than DFT, GFT, and WT.

Similarly, in Gaussian noise, as shown in Figure 2.4, the SNRs of the filtered signals with l_1 -norm and l_2 -norm GFT decrease at a high intensity of Gaussian noise (SNR=-5dB), while the SNR of the filtered signal with GFT improves after denoising high intensity of Gaussian noise (SNR=5dB). These results indicate that GFT may deteriorate the signal quality in strong noisy environments and fail to achieve the purpose of denoising. This may be due to the fact that the estimation of the underlying graph where the signals reside relies on the signal itself rather than the actual distance between the leads. The deterioration of the signal leads to a serious failure of the estimation of the adjacency matrix. In this case, the main energy of the signal is concentrated in the noisy channel, and the edge weights between the noisy channel and the rest of the channels cannot be estimated accurately. As a result, the noise cannot be filtered out by GFT. DFT (temporal smoothing), on the other hand, is more robust to Gaussian noise compared to wavelet transform. Thus, GFT can further take effect in denoising after the DFT has effectively suppressed the noise, resulting in an overall higher SNR of JFT. Although the WT can suppress Gaussian noise well, it has little or no suppression effect on impulse noise. This may be due to the fact that the wavelet coefficients of impulsive noise after wavelet transform are concentrated and not lower than those of the actual EEG signal. It is worth noting that DFT1 imposes more similar to a linear constraint on the EEG signal. When the parameters are not properly chosen, as shown in Figure 2.4, the EEG signal within the small window is more similar to linear, which we believe is not in line with the characteristics of the EEG signal and may interfere with the subsequent feature extraction of the EEG signal. Thus, we recommend DFT2 for EEG noise reduction compared to DFT1.

And as for spontaneous noise, to reveal the results of Figure 2.5(b), the signal waveform at noise intensity of SNR=-5dB is drawn in Figure 2.6. We found that the ERP signal has been completely submerged in the resting EEG, and all the algorithms are unable to extract the P300 signal. At SNR=5dB, as shown in Figure 2.5(a), the role of GFT is more similar to that of PCA in extracting the main components of the EEG signal. In general, the signal power is more concentrated in the lower frequencies of the graph, which also captures the vast majority of the signal's features. This is the main reason why GSP are currently used for dimensionality reduction(Kalantar, Sadreazami, Mohammadi,

& Asif, 2017; Rui, Nejati, & Cheung, 2016). Previously, Rué-Queralt found that the connectome harmonics decomposition provided by graph spectral theory may be superior to techniques such as PCA and ICA in dimensionality reduction. The study in this thesis implies that reconstruction of the signal with low-dimensional harmonics preserves the main features and suppresses some of the noises. However, the denoising performance of GFT will be greatly affected by the estimation of the graph structure. Thus, the development of a stable estimation method of the underlying graph structure may be more beneficial for the subsequent application and development of denoising algorithms based on graph spectral theory.

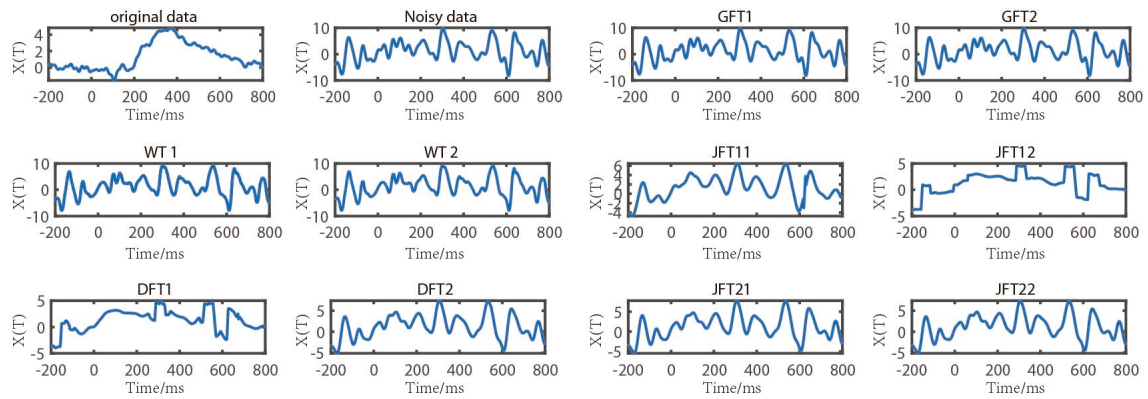


Figure 2.6 Signal waveform when SNR=-5dB (the intensity of spontaneous EEG noise)

To explore the improvement of decoding efficiency of EEG signals after JFT denoising, we constructed classifiers using SWLDA for the data before and after denoising. In dataset 1, we classified auditory hallucinations with schizophrenia and healthy controls and found that the classification accuracy after JFT21 filtering was as high as 82.69%. In dataset 2, the character recognition accuracy of the P300 speller after JFT22 denoising is as high as 100% when the number of repetitions is 5. Besides, the computation time of JFT22 is much smaller than that of WT. The classification experiments in the P300 dataset verify the effectiveness of the algorithm and favorably support the hypothesis that the combination of temporal and spatial constraints can suppress the noise better.

Overall, graph spectral theory can remove noise based on the dependencies between different channels of the EEG signal. Considering the low spatial resolution and high temporal resolution of EEG signals, the pure graph filter method may not be sufficient to deal with complex noises. Thus, we introduce temporal smoothing and develop the JFT methods. The results of simulation and classification experiments show that JFT has

better performance in suppressing various noises compared with traditional wavelet transform and other methods, and can effectively improve the decoding accuracy of disease models and brain-computer interface.

2.6 Conclusion

In this chapter, we focus on the performance of denoising algorithms based on graph spectral theory. We combine the graph domain-informed constraints with the temporal smoothing constraints, develop a JFT algorithm, and further explore the effectiveness of the algorithm in simulation experiments and classification experiments. We find that the denoising algorithm under the joint constraints can effectively suppress impulse noise, Gaussian noise, and spontaneous EEG noise, enhance the decoding efficiency, and improve the efficiency of the classification. However, the poor performance of the GFT at high intensity of impulse and Gaussian noise reminds us that the effectiveness of the estimation of the underlying graph structure will greatly affect the performance of the GFT. Although the estimation of the graph structure has not been deeply explored at present, the experimental results still demonstrate the effectiveness of the graph spectral theory based on the joint time-vertex framework, which provides new insight for the development of denoising algorithms for EEG signals based on graph spectral theory. In addition, although graph spectral theory has been increasingly used in denoising and feature extraction in cognition and disease research, further exploration is needed regarding the relationship between graph spectral features, cognition and EEG rhythms.

Chapter 3 Analysis of Schizophrenia Based on Graph Spectral Theory

3.1 Abstract

In the previous chapter, we focused on the application of graph spectral theory to denoise EEG. In this chapter, we will delve into the main reasons why graph spectral theory can be used for denoising. The relationship between graph harmonics and EEG rhythms will be further discussed in depth in this chapter. In previous studies, researchers have found that connectome-harmonic decomposition (CHD) analysis based on graph spectral theory provides a natural distribution pattern of connectomes and is an effective tool for analyzing the coupling of structural networks and functional signals as well as cortical network dynamics. Therefore, in this section, we will explore the application of CHD analysis based on graph spectral theory in schizophrenia.

Abnormalities in brain network dynamics in schizophrenia have now been widely reported. For SCZ, researchers have now mainly explored the brain network connectivity changes in SCZ patients as well as ERP components. However, few researches have been carried out to explore the neural mechanism changes in schizophrenia from the perspective of the coupling of structural and functional signals. So, this study may fill the gap in this part of the study. On the other hand, current studies of schizophrenia have focused on the P300 component of the ERPs but have rarely investigated the activation patterns of different EEG rhythms from the source space and their relationship with neurocognitive alterations. In addition, the relationship between brain rhythm alterations of SCZ patients and graph harmonics needs to be further elucidated. Therefore, this thesis combines the power spectral density and graph spectral theory to explore the differences between the two groups of subjects in the brain activation of low-frequency graph harmonic and high-frequency graph harmonic and their relationship with neurocognition. This will further provide new analytical techniques and a research basis for the exploration of the neurophysiological endophenotypes of schizophrenia. In addition, the difference in cognitive patterns captured by low-frequency and high-frequency graph harmonics will further support and demonstrate the reliability of graph harmonics for dimensionality and graph filters.

3.2 Introduction

SCZ is one of the most common and disabling psychiatric disorders. Thus, finding objective neurophysiological endophenotypes and exploring their relationship with neurocognitive alterations play an important role in understanding the neural mechanisms of SCZ, diagnosis, and assessment of treatment effects. The Schizophrenia Genetics Consortium examined the genetic basis of neurocognitive biomarkers in families with a high prevalence of SCZ and identified candidate endophenotypes related to attention, working memory, and verbal declarative memory (Gur et al., 2007). Antonova et al. investigated structural-neurocognitive relationships in SCZ and found that the prefrontal cortex, temporal lobe, hippocampus, and parahippocampal gyrus were highly correlated with neurocognitive levels (Antonova, Sharma, Morris, & Kumari, 2004). In EEG, researchers mainly found prepulse inhibition deficits in SCZ patients (Swerdlow et al., 2014), loss of oculomotor nerve during counter scanning (Levy et al., 2004), mismatch negativity (MMN) (Levy et al., 2004), and P300 deficits in SCZ patients (Bramon, Rabe-Hesketh, Sham, Murray, & Frangou, 2004). These deficits are highly correlated with neurocognitive deficits such as attention. In addition to this, dysfunctions in EEG rhythms in SCZ patients have been widely reported. δ and θ as the most basic components of the P300, usually show a tendency to be decreased in SCZ patients (Schmiedt, Brand, Hildebrandt, & Basar-Eroglu, 2005). However, γ activity is influenced by the behavioral state of schizophrenia and the difficulty of tasks and shows either an increased or an attenuated tendency (Başar & Güntekin, 2008). Specifically, patients with a working memory load (Kedzior & KMathes, 2007) or positive symptoms (Schmiedt et al., 2005) usually show increased gamma amplitude. These studies have explored the SCZ abnormalities and their relationship with neurocognitive activities, mainly in terms of EEG rhythms and gray matter in local brain regions. However, as a highly interconnected system, the brain accomplishes cognitive functional activities mainly through complex modulations across multiple brain regions. Classical signal processing methods in the time and frequency domains are not sufficient to decode the cognitive activities of the brain. As a result, complex network analysis methods have been widely noticed and used in disease research.

Graph spectral theory is an effective means of analyzing complex networks and an emerging tool for describing the fundamental characteristics of the interactions between multiple brain regions. It can be used to filter functional signals such as fMRI (Medaglia

et al., 2018), extract features (Pilavci & Farrugia, 2019), decode of cognitive processes (Prete & Van De Ville, 2019) and neurological disorders (Jestrović, Coyle, & Sejdić, 2017), as well as explore the structure-function relationships. Unlike previous techniques for exploring brain dynamics, the connectome-harmonics used in this thesis rely exclusively on structural connectivity and can be used as a generalized, anatomical harmonic representation for any functional signals. It is analogous to the decomposition of signals by Fourier transforms using sine and cosine functions. In previous studies, researchers have found that brain oscillations can be categorized into δ , θ , α , β , and γ waves according to their frequency bands and that different waves support different modes of information processing (Fries, 2015). A more recent study by Vezoli has shown that white matter anatomy limits oscillatory activity in different frequency bands (Vezoli et al., 2021). Studies of brain network dynamics have shown that low-frequency oscillations are more likely to modulate long-range interactions and high-frequency oscillations are more likely to modulate short-range localized activity. This result was demonstrated by CHD analysis (Rué-Queralt et al., 2021; Rué-Queralt et al., 2023) which further suggests that CHD analysis may become an important tool for subsequent studies of structural and functional coupling. Indeed, the CHD method was later used for the estimation of functional networks in resting-state states by Atasoy (Atasoy et al., 2017). Besides, it has since been widely used in the study of disorders such as autism spectrum disorders (Brahim, Hajjam El Hassani, & Farrugia, 2019), and ADHD (Y. Li & Mateos, 2019). Local and distributed functions of the brain coexist, and CHD emphasizes viewing brain activity in terms of connectome harmonics (distribution patterns at different spatial scales). Thus, CHD analysis is just as reasonable as viewing it in terms of discrete spatial locations (Luppi et al., 2023).

Numerous reports elucidated the changes in brain network dynamics of SCZ patients and suggested that these abnormal network dynamics should be responsible for the neurocognitive deficits in SCZ patients. Farzan et al. found that cognitive deficits may be caused by abnormal connectivity between frontal, temporal, and parietal regions in patients with schizophrenia (Farzan et al., 2010). Stotesbury found that reduced processing speed was associated with white matter abnormalities that are widespread across brain regions (Stotesbury et al., 2018). Eryilmaz et al. reported that the degree centrality of the brain network in the prefrontal and parietal lobes was associated with working memory and was a valid predictor of working memory test scores of SCZ

patients (Eryilmaz et al., 2022). Studies have revealed structural or functional network abnormalities between different brain regions of SCZ patients. However, few researchers have revealed changes in the coupling of structural network and function signal in SCZ patients and their relationship with cognitive impairment. In this thesis, we introduced the CHD analysis to reveal the changes in cortical network dynamics during P300 in SCZ, the activation changes in different EEG rhythms at low-frequency and high-frequency graph harmonics, and their associations with neurocognition. Our research will provide a new way of the exploration of the neurophysiological endophenotypes of SCZ.

3.3 Data and Processing Flow

3.3.1 Data

The research data were collected and provided by the B-SNIP (Clementz et al., 2016). The schizophrenia (N=147), as well as healthy controls (HC) (N=200), underwent clinical characterization and brief assessment of schizophrenia cognition (BACS). Healthy controls were identified based on their family history; they and their first-degree relatives must have no history of psychiatric disorders. All participants underwent EEG recording with a sampling rate of 1000Hz and 64 electrodes. Additionally, to elicit event-related potentials, the auditory oddball paradigm was applied. During the collection process, participants sat in soundproof booths and listened to tones emitted from two 8 Ω speakers positioned 50 centimeters in front of them. The stimuli consisted of 567 standard tones (1000 Hz) and 100 target tones (1500 Hz), presented in a pseudorandom order with a trial interval of 1300 milliseconds. Participants were instructed to press a button when they detected a target tone.

3.3.2 Data Processing Flow

Figure 3.1 illustrates the data acquisition and processing of EEG signals in this study. As shown in Figure 3.1(a), SCZ patients and healthy controls had completed the neurocognitive tasks and scores, and their task-state P300 EEG had been acquired. After that, to ensure the reliability of the results, we first pre-processed the data with eeglab. As shown in Figure 3.1 (b), the EEG signals were firstly filtered by a 0.5-45Hz bandpass filter, then REST reference was used for zero potential estimation, followed by removing muscle artifacts and electromyographic artifacts by ICA. After that, the ERP is extracted

based on the label information, at which time the trial with EEG amplitude higher than 120uV will be identified as an artifact, and the trial will be discarded.

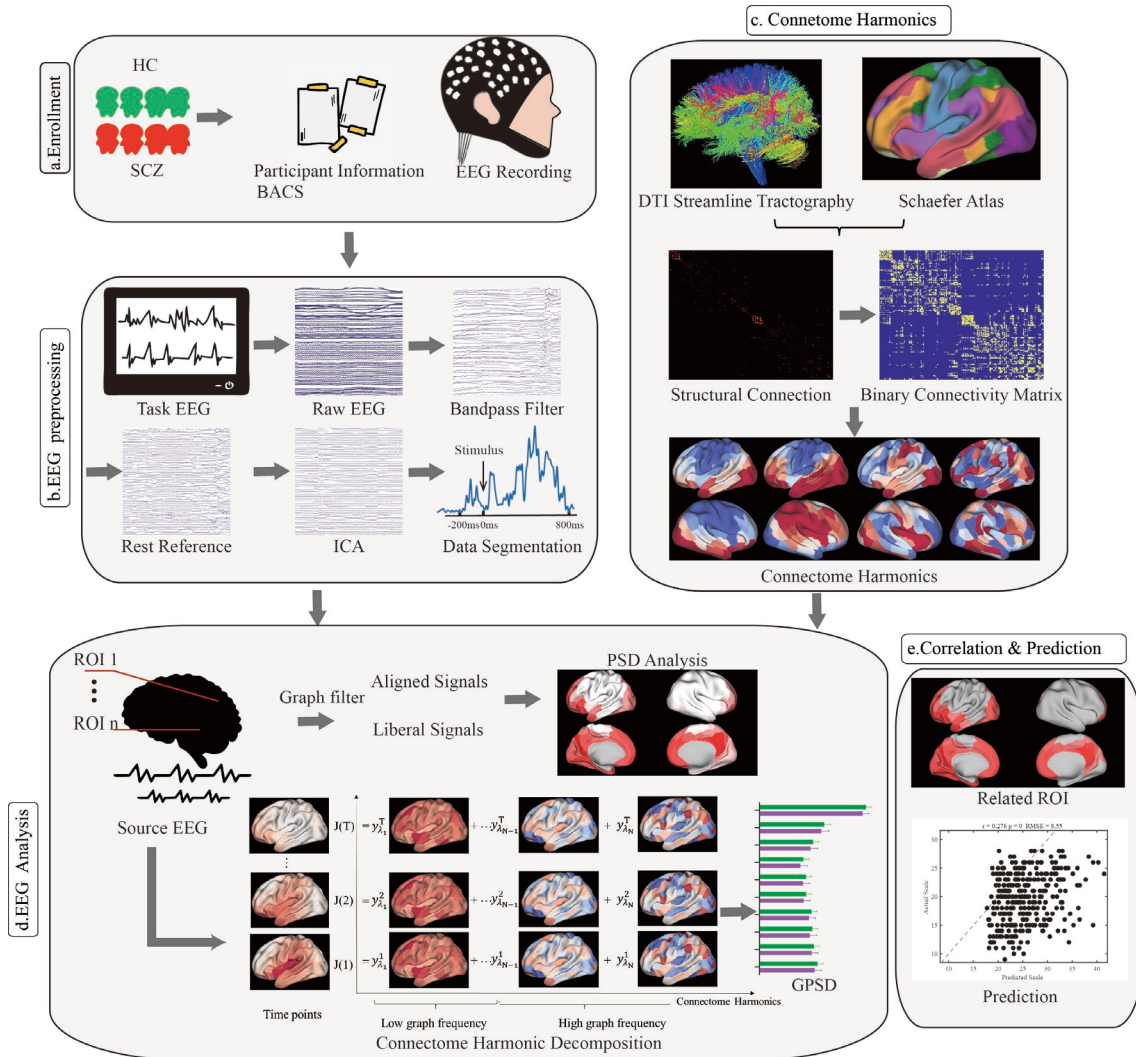


Figure 3.1 Flowchart of data analysis based on graph spectral theory

Before applying CHD analysis, we need to construct the connectome harmonics through the process shown in Figure 3.1 (c). Firstly, we obtain the structural brain network through DTI images. Then to ensure the portability of the structural network in SCZ patients and healthy controls, we keep only the first 13% of the connections and obtain the connectome harmonics by constructing the Laplace matrix. After obtaining the connectome harmonics, as in Figure 3.1 (d), we averaged the scalp ERP over all trials and traced them back to the cortex, followed by extracting the source activity of 200 ROIs according to Schaefer's template. At this point, we had access to the connectome harmonics and the EEG signals residing on these networks, thus allowing us to perform

a CHD analysis. We first analyzed the graph spectral power density of EEG signals at different graph harmonics. After that, to further explore the relationship between graph harmonics and rhythms, we filtered the signals into graph high-frequency and low-frequency signals and analyzed their PSD to find the cortex activation at different graph harmonics. As shown in Figure 3.1 (e), the extracted features are correlated and predicted with the collected BACS scales to understand the relationship between graph harmonics and neurocognitive abilities.

3.4 Methods

In the previous part, we introduced the main technical routes of this chapter. In this section, we will specifically introduce the methods used in this chapter, which mainly include source localization techniques, construction of consensus structural brain networks, graph power spectral density, and power spectral density.

3.4.1 Source Localization Techniques

Here, we used standardized low resolution brain electromagnetic tomography (sLORETA) to reconstruct cortical source signals from scalp EEG. As shown in Eq.(3-1), sLORETA assumes that the scalp EEG $\phi \in R^{E \times 1}$ can be obtained from the current density $J \in R^{3V \times 1}$ in the cortex with a certain weight, and the weight transfer matrix is $K \in R^{E \times (3V)}$, and V is the number of sources. Besides, the acquired signal will also be susceptible to noise in the natural environment and other noise interference. The noise signal is represented by $\varepsilon \in R^{E \times 1}$. To obtain the solution of Eq. (3-1), we can solve the minimization problem shown in Eq. (3-2), where α is the regularization parameter.

$$\phi = KJ + \varepsilon \quad (3-1)$$

$$\arg \min_J \|\phi - KJ\|^2 + \alpha \|J\|^2 \quad (3-2)$$

The solution of the problem is as follows:

$$\hat{J} = T\phi \quad (3-3)$$

$$T = K^T [KK^T + \alpha H]^+ \quad (3-4)$$

where $H \in R^{E \times E}$ is the centroid matrix and $+$ is Moore–Penrose pseudoinverse.

Ultimately, by normalizing \hat{J} with Bayesian theory, we obtain the solved current density for the l th voxel as shown in the following Eq.(3-5), where $S_{\hat{J}}$ is the variance of the estimated normalized current density.

$$P_l = \hat{J}_l \left\{ \left[S_{\hat{J}} \right]_{ll} \right\}^{-1} \hat{J} \quad (3-5)$$

$$S_{\hat{J}} = K^T [KK^T + \alpha H]^+ K \quad (3-6)$$

After obtaining the source EEG, we obtained 200 ROIs' locations based on the 2018 Schaefer template, and then found the corresponding voxels in each ROI. Then, the source activities for voxels within each ROI are averaged to obtain the source EEG activity for each ROI.

3.4.2 Construction of Consensus Structural Brain Networks

To obtain connectome harmonics, we obtained consensus connectivity matrices from the publicly available DTI database from the Human Brain Connectome Project. The dataset contained a total of 400 healthy subjects (170 males; age range 21-35 years). Next, we performed DTI preprocessing of the DTI images using FMRIB software with MRtrix3 and Freesurfer. First, the Eddy function of FSL was used to correct the DTI images for motion. Then, to attenuate each isotropic diffusion in the cerebral white matter and to provide more accurate fiber orientation information, we used constrained spherical deconvolution to estimate the multi-shell and multi-tissue response function. Then, the FAST algorithm was used to segment the T1w-weighted images that had been registered to the b0 volume. With anatomically constrained traction, the second-order integration of the fiber orientation distribution was performed to generate an initial traction map with 10 million streamlines. The spherical deconvolution (SIFT2) method was then applied to informally filter the traction map to provide a more accurate metric of biofiber connectivity. Finally, an anatomical connectivity matrix was obtained based on the definition of the 200-region atlas provided by Schaefer. Finally, after averaging the network adjacent matrices across all subjects, to ensure the stability of the filtered structural connections across all subjects (healthy controls and SCZ patients), we retained only the top 13% of the connections in the DTI matrix and further binarized them. As a result, we obtained the consensus binary DTI network matrix between these 200 ROIs.

3.4.3 Graph Power Spectral Density

Now, the consensus matrix $W \in R^{N \times N}$ is obtained. We then obtain the normalized Laplace matrix by the following Eq. (3-8) and Eq. (3-9), where $D \in R^{N \times N}$ is the diagonal matrix which can be obtained from Eq. (3-7). By decomposing the matrix in Eq. (3-10), we can obtain the basis of the graph Fourier transform $U = [u_1, \dots, u_N] \in R^{N \times N}$, which is also referred as the connectome harmonics. Λ is the diagonal matrix, where λ_d is the eigenvalue of the Laplace matrix which characterizes the smoothness of the graph connectivity harmonics over the graph. In general, low-frequency harmonics correspond to smaller λ_d , slower variation patterns on the graph, and coarse-grained spatial variation patterns. High-frequency harmonics correspond to larger λ_d , faster variation of the signal on the graph, and fine-grained spatial variation patterns.

$$D(ii) = \sum_{i=1}^N W_{ij} \quad (3-7)$$

$$L = D - W \quad (3-8)$$

$$L_{norm} = D^{-\frac{1}{2}} L D^{-\frac{1}{2}} \quad (3-9)$$

$$L_{norm} = U \Lambda U^T \quad (3-10)$$

From the above equations, we obtain the connectome harmonics U . Now, we can quantify how brain activity is constrained by this underlying structural network through the Graph Fourier Transform (GFT). By connectome harmonics matrix U , we can re-express the EEG source signal at the i th ROI and time t , as shown in Eq. (3-11). y'_i measures the degree to which the signal is constrained by the structural connections. $Y^t = [y'_1, \dots, y'_N]$ is the graph Fourier coefficient which can be obtained from the GFT as shown in Eq.(3-11)

$$Y^t = U^T J^t \quad (3-11)$$

Finally, to obtain the graph power spectral density (GPSD), we refer to the method used by Rue-Queralt to regularize the graph Fourier coefficients Y^t for each subject (Rue-Queralt et al., 2021). The GPSD of each harmonic at time point t is then obtained by using the following Eq. (3-12), which represents the activation of the connectome harmonics at time point t . Usually, the activation of low-frequency connectome harmonics corresponds to the activation of the information integration mode, while the activation of high-frequency harmonics corresponds to the activation of the information segregation mode.

With GPSD, we can observe changes in the brain dynamics (integration or segregation) at the ms level.

$$GPSD(u_d, t) = |y_\lambda^t|^2 \quad (3-12)$$

3.4.4 Power Spectral Density

We will obtain aligned signals (corresponding to the graph low-frequency signal) and liberal signals (corresponding to the graph high-frequency signal) through graph filters to further understand their role in contributing to the EEG rhythms. The first k connectome harmonics that capture 50% of the graph energy are recognized as the low-frequency harmonics and the rest harmonics as the high-frequency harmonics, where we choose k to be 4. Next, we can construct the low-frequency graph filter by Eq. (3-13) and Eq. (3-14). Subsequently, the low-frequency aligned signals can be obtained by Eq. (3-16). Similarly, the graph high-frequency filter is constructed by Eq. (3-13) and Eq. (3-15), and then the high-frequency liberal signal is obtained by Eq. (3-17).

$$F = \text{diag}(f(\lambda_0), \dots, f(\lambda_{n-1})) \quad (3-13)$$

$$f_L(\lambda_k) = \begin{cases} 1, & \text{if } k \in \{0, \dots, 4\} \\ 0, & \text{otherwise} \end{cases} \quad (3-14)$$

$$f_H(\lambda_k) = \begin{cases} 0, & \text{if } k \in \{0, \dots, 4\} \\ 1, & \text{otherwise} \end{cases} \quad (3-15)$$

$$J_i^{\text{aligned}} = UF_L U^T J_i^t \quad (3-16)$$

$$J_i^{\text{liberal}} = UF_H U^T J_i^t \quad (3-17)$$

Then we calculate the power spectral density of SCZ patients and healthy controls at each ROI by the average periodogram method Welch. The signal sequence $x(t)$ contains N sampling points, and it can be divided into L segments. The coverage between the i th and $i-1$ th segments is 50%. Assuming that the signal of i -th segment is $x_i[n]$, its periodogram $P_s^{(i)}(f)$. and the corrected periodogram $P_w^{(i)}(f)$ can be obtained by the following Eq. (3-18) and Eq. (3-19), where $w[n]$ (the Hamming window) is mainly used to solve the problem of spectrum leakage.

$$P_s^{(i)}(f) = \frac{1}{L} \left| \sum_{n=1}^{L-1} w[n] x_i[n] e^{j2\pi f n} \right|^2 \quad (3-18)$$

$$P_w^{(i)}(f) = \frac{1}{M} \left(\sum_{i=1}^M P_S^{(i)}(f) \right) \quad (3-19)$$

Now, we can obtain the PSD distributions of the graph low-frequency signal $J^{aligned}$ and graph high-frequency signals $J^{liberal}$ at different ROIs.

3.4.5 Correlation and Regression Prediction Analysis

In order to further explore the neural mechanisms of cognitive impairment in SCZ patients, we expected to find potential relationships between the above features and cognitive scales to find the neurophysiological endophenotypes of SCZ. We used Pearson correlation analysis to calculate the correlation between the GPSD of the source EEG signals and the distribution of the PSD of the graph low-frequency and high-frequency signals with the cognitive scales, respectively. We then constructed a prediction model to predict cognitive task scores using the EEG activation of aligned signal in δ -wave. The prediction model is as follows:

$$AR = \beta_0 + \beta_1 P_1 + \beta_2 P_2 + \dots + \beta_m P_m + \varepsilon \quad (3-20)$$

where AR denotes the specific cognitive task score, $P_{1\dots m}$ denotes the PSD for m ROI, ε is the error term, and $\beta_{0\dots m}$ is the regression coefficient.

The cross-validation strategy of leave-one-out is used to partition the training and test sets. For n samples, in each cross-validation, $n-1$ samples are used as the training set, and one remaining sample is used as the test sample. Based on the PSD and cognitive task scores of these $n-1$ samples, a prediction model was constructed to predict the cognitive scores of the rest. This process was repeated n times until all samples were used as a test sample. Next, to measure the predictive performance of the predictive model, Pearson's correlation was used to assess the correlation coefficients between the subjects' actual cognitive task scores and the predicted cognitive task scores. Meanwhile, root mean square error (RMSE) was used to measure the prediction error, which is defined as follows:

$$RSME = \sqrt{\frac{1}{N} \sum_{i=1}^N (X_i - Y_i)^2} \quad (3-21)$$

where N is the number of samples, X is the observed value, and Y is the predicted value. The smaller the RMSE, the higher the correlation coefficient, and the more effective the predictive model.

3.5 Results

In this section, we will focus on the findings of this chapter. Firstly, we'll introduce the cognitive scales and ERP. The change of P300 of SCZ is the most reproducible result at present, which will provide the basis for the reliability of our data and pre-processing. Then we will present the results of the graph harmonic analysis, focusing on the change of GPSD and EEG rhythms on different graph harmonics for SCZ patients, and explore the relationship between these features and neurocognitive scales, to reveal the associations between cortical graph harmonic changes and neurocognitive deficits of SCZ patients.

3.5.1 Cognitive Scales and ERPs

Figure 3.2 (a) below illustrates the scores obtained by SCZ patients and the healthy subject group in various cognitive tasks after undergoing the BACS cognitive assessment. We found that the SCZ patients obtained much lower scores than the healthy subjects in all of these experiments in the Digital Sequencing, Symbol coding, Tower of London, Token Motor, Verbal Memory, and the Animal Naming Test ($p < 0.01$; FDR corrected). Figure 3.2 (b) shows the ERP waveforms of SCZ patients and healthy controls. We found that the evoked EEG amplitude of SCZ patients was significantly lower than the evoked EEG amplitude of the healthy control group during P300 ($p < 0.01$; FDR corrected).

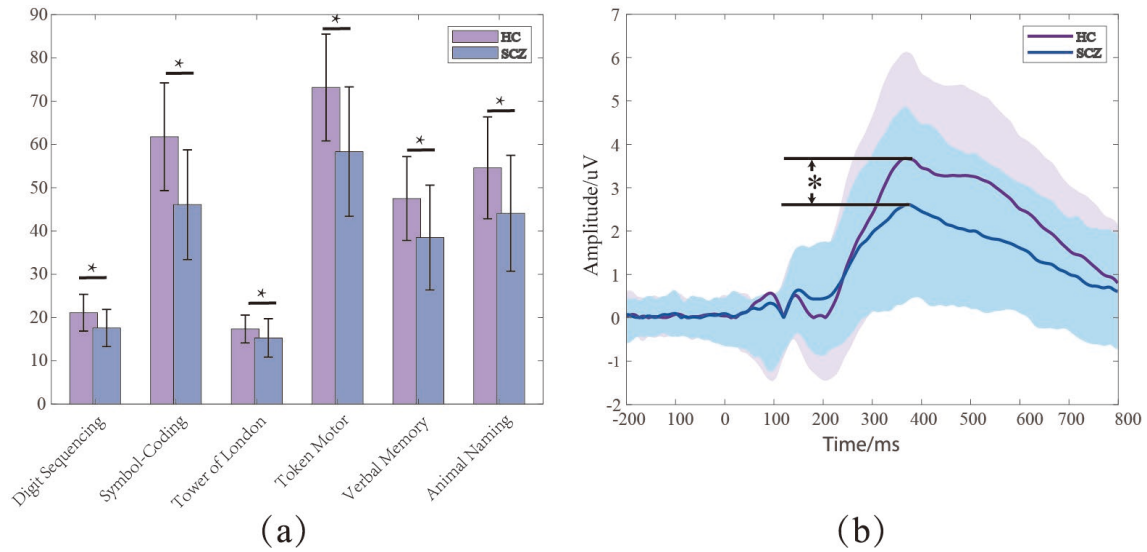


Figure 3.2 Cognitive scale scores and ERP waveforms for two groups of subjects. (a) Differences in cognitive task scores of two groups (*: $p < 0.01$ by T-test). The error bar represents the standard deviation; (b) Evoked ERP waveforms of healthy subjects and SCZ patients (*: $p < 0.01$ by T-test).

3.5.2 GPSD

Next, we calculated and compared the total GPSD and the GPSD on each connected harmonic of the two groups of subjects during P300. As shown in Figure 3.3 (a) below, the total GPSD of SCZ patients was significantly lower than that of the healthy control group. After that, we divided the 200 harmonics evenly into 10 groups and obtained the summed GPSD on each set of harmonics for the healthy subjects and the schizophrenic patients. As shown in Figure 3.3 (b), we can find that the GPSD of SCZ patients is significantly lower than that of the healthy control group ($p < 0.01$; FDR corrected) on all the binned harmonics, which represent different spatial distributions. The top of Figure 3.3 (b) shows the energy distribution of each set of harmonics. What we can observe is that the energy of the first harmonic tends to be more globally smoothed, whereas the last 9 harmonics tend to be more locally distributed compared to the first harmonic.

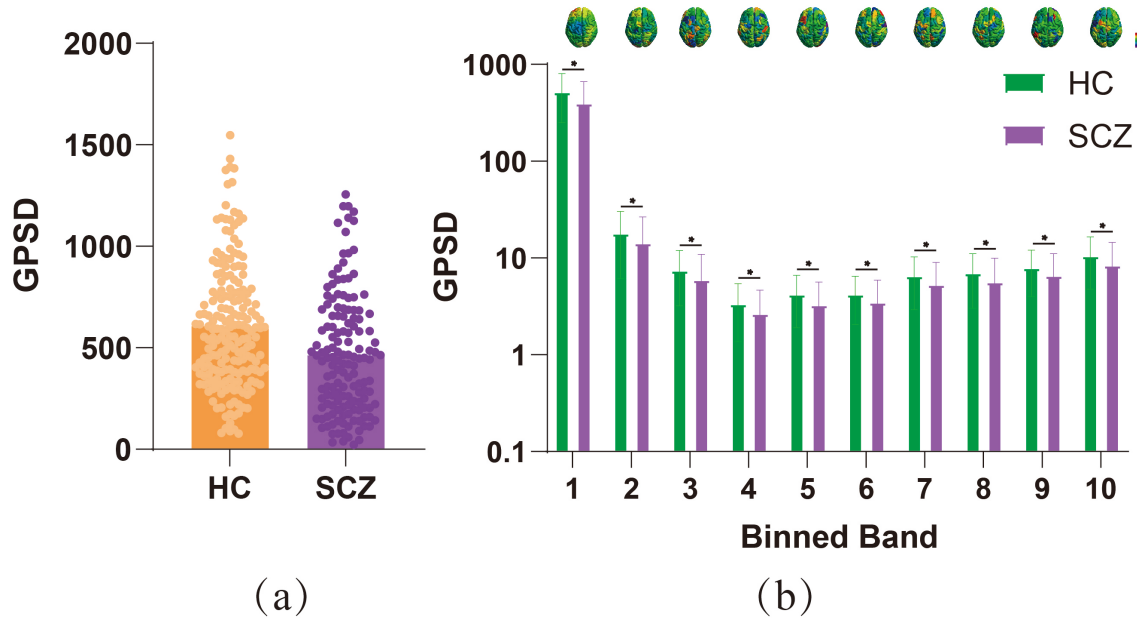


Figure 3.3 Total harmonic energy alteration and alteration of harmonics at different scales. (a) Total GPSD for all harmonics for two groups; (b) Distribution of GPSD at 10 sets of harmonics and their differences between the two groups (*: $p < 0.01$ by T-test)

To further understand the differences in different EEG rhythms at different spatial scales, we obtained the low-frequency aligned signals and the high-frequency liberal signals and analyzed their PSD distributions. As shown in Figure 3.4 below, we can see that for the aligned signals, the differences in the PSD distributions of HC and SCZ patients are mainly concentrated in the δ , β , and γ bands. Specifically, in the δ band, the activation of SCZ patients in the frontal, occipital, and temporal lobes was significantly lower compared to that of the healthy controls; whereas, no differences between SCZ patients and the healthy controls were seen in the θ - and α -frequency bands; in the β -frequency band, we observed that the brain activation of SCZ patients in the right temporal lobe, occipital lobe, and other regions was significantly lower than that of the healthy controls; in the γ -frequency band, the differences in PSDs between two groups were mainly centered on right occipital lobe, parietal lobe and temporal lobe ($p < 0.01$, FDR corrected). For the graph high-frequency signals, the differences in PSD between HC and SCZ patients were mainly concentrated in the β and γ bands. Specifically, in the β -band, the brain activation of SCZ patients was stronger in the right temporal lobe and occipital lobe than in the healthy control group; in the γ -band, we could find that the brain regions with increased activation were almost the same as those in the β -band.

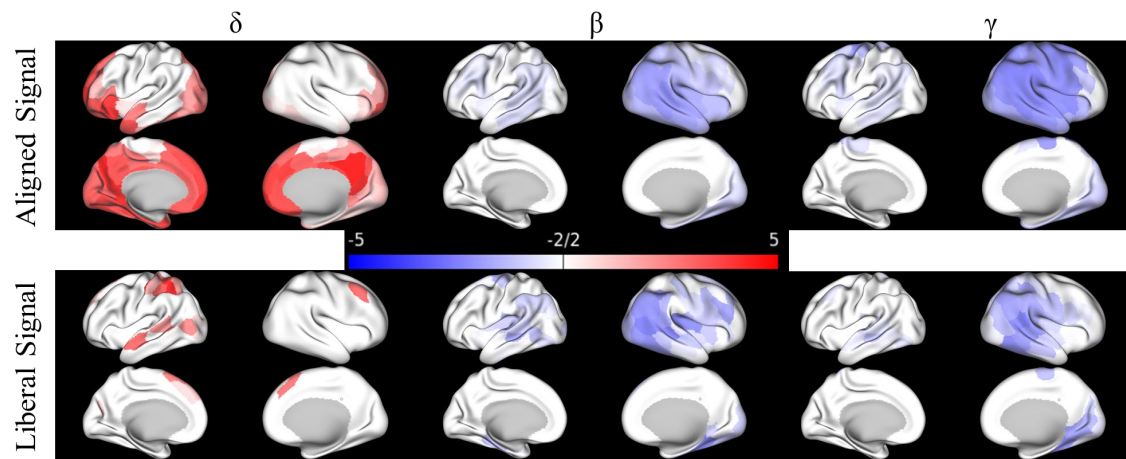


Figure 3.4 T-value topographic maps of the statistical difference in PSD between the aligned signal and the liberal signal for healthy controls and the SCZ patients ($p < 0.01$ by T-test). The red color represents higher activation in the region of healthy subjects and the blue color represents higher activation in the region of SCZ patients

3.5.3 Correlation and Prediction Results

To verify the relationship between changes in brain network dynamics and cognitive changes, we analyzed the relationship between GPSD and cognitive scale scores of the two groups of subjects and found that GPSD showed significant positive correlations with scores on all cognitive tasks during P300, as shown in Figure 3.5 below. Specifically, scores on the digit sequencing task were positively correlated with GPSD ($r = 0.207, p < 0.01$); scores on the symbol-coding task were positively correlated with GPSD ($r = 0.3, p < 0.01$); scores on the Tower of London task were positively correlated with GPSD ($r = 0.207, p < 0.01$); scores on the token motor task were positively correlated with GPSD ($r = 0.238, p < 0.01$); scores on the animal naming task were positively correlated with GPSD ($r = 0.242, p < 0.01$); and scores on the verbal memory scores were positively correlated with GPSD ($r = 0.273, p < 0.01$).

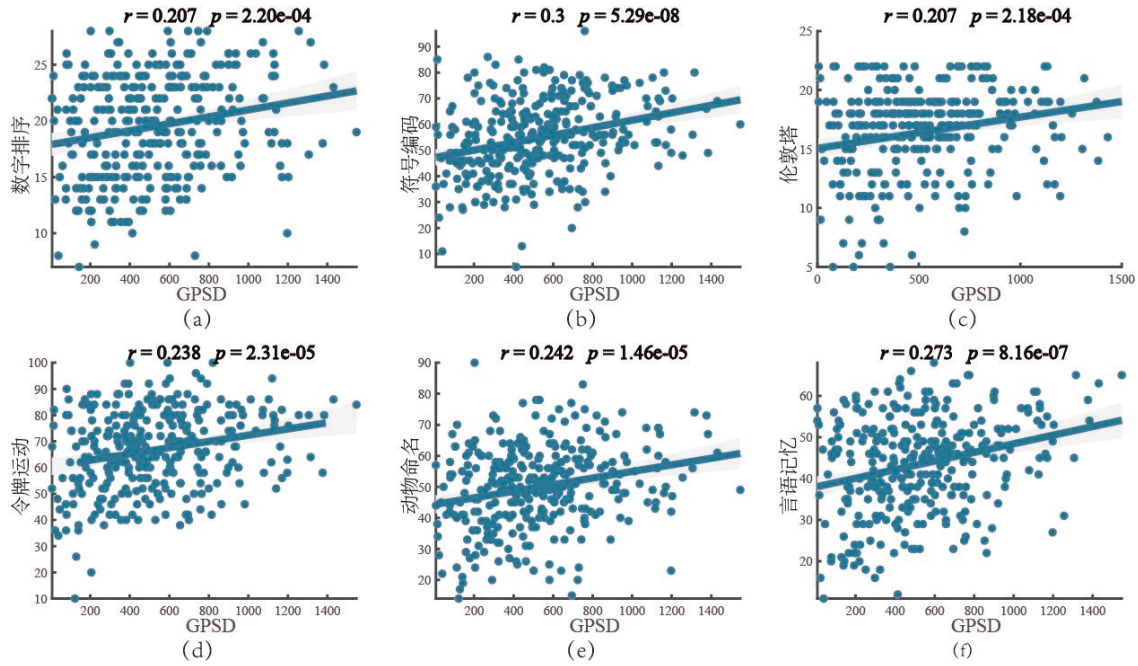


Figure 3.5 Relationships between total GPSD and individual scores on cognitive tasks for two groups of subjects (by Pearson correlation). (a) Digit sequencing task; (b) Symbol-coding task; (c) Tower of London task; (d) Token motor task; (e) Animal naming task; (f) Verbal memory scores.

As shown in Figure 3.4, the graph low-frequency captures most of the different EEG rhythms between the two groups. Then, to verify whether the alteration in PSD in graph low-frequency is associated with cognitive impairment, we do correlation and prediction analysis with the cognitive scales. Figure 3.6 and Figure 3.7 illustrate the correlation results between PSD of the δ and γ bands in graph low-frequency and cognitive scales. In the δ and γ bands, the brain regions that showed strong correlations with the cognitive scales were essentially the same as those presented in Figure 3.4 where activation differences existed ($p < 0.01$). Specifically, PSD in the frontal, temporal, and occipital cortex in the δ frequency band all showed a significant positive correlation with scores on the six cognitive tasks; activation in the parietal lobe in the γ frequency band, on the other hand, showed a negative correlation with scores on the cognitive tasks.

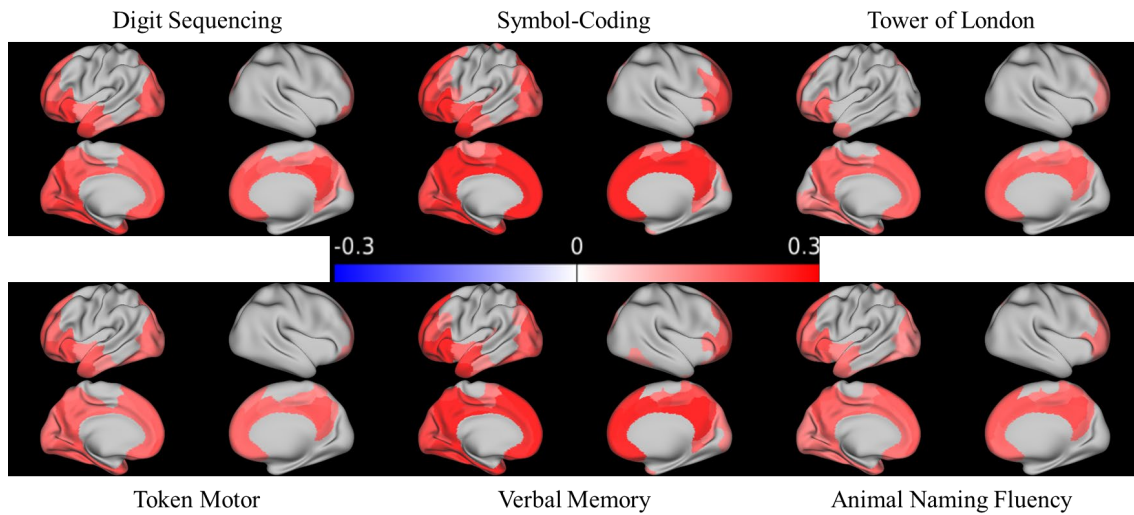


Figure 3.6 R-value topographic maps of relationships between PSD of aligned signals for the δ -band and scores on tasks such as digit sorting, symbol encoding, Tower of London, token movement, verbal memory, and animal naming

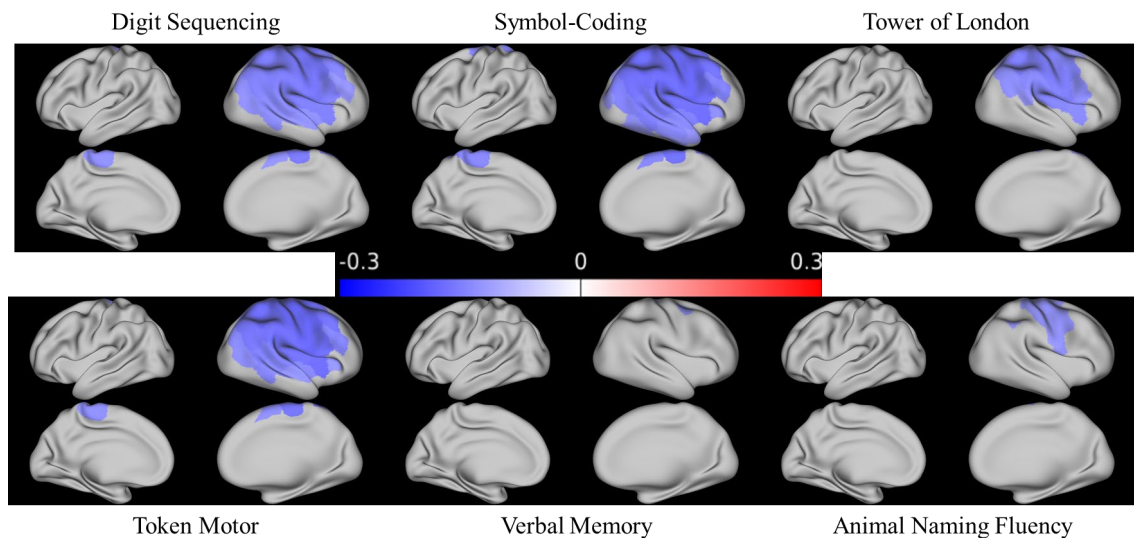


Figure 3.7 R-value topographic maps of relationships between PSD of aligned signals for the γ -band and scores on tasks such as digit sorting, symbol encoding, Tower of London, token movement, verbal memory, and animal naming

From Figure 3.6, we can find that PSD in the δ band of aligned signal has a great relationship with neurocognition, which suggests that the activation in the δ band may capture the key brain regions of cognitive deficits in SCZ patients. To further validate our

hypothesis, we next utilized the PSD of aligned signals to predict the cognitive task scores. The results are shown in Figure 3.8, where the black solid dots represent individual subjects and the dashed diagonal line represents the ideal prediction state. We can find that in all six tasks, the predicted task scores are positively correlated with the actual observed task scores, and the values are significantly less than 0.01. In particular, compared to the scores of the other four tasks, we were able to predict better for the scores of the two tasks, symbol encoding and verbal memory with PSD of the δ -band.

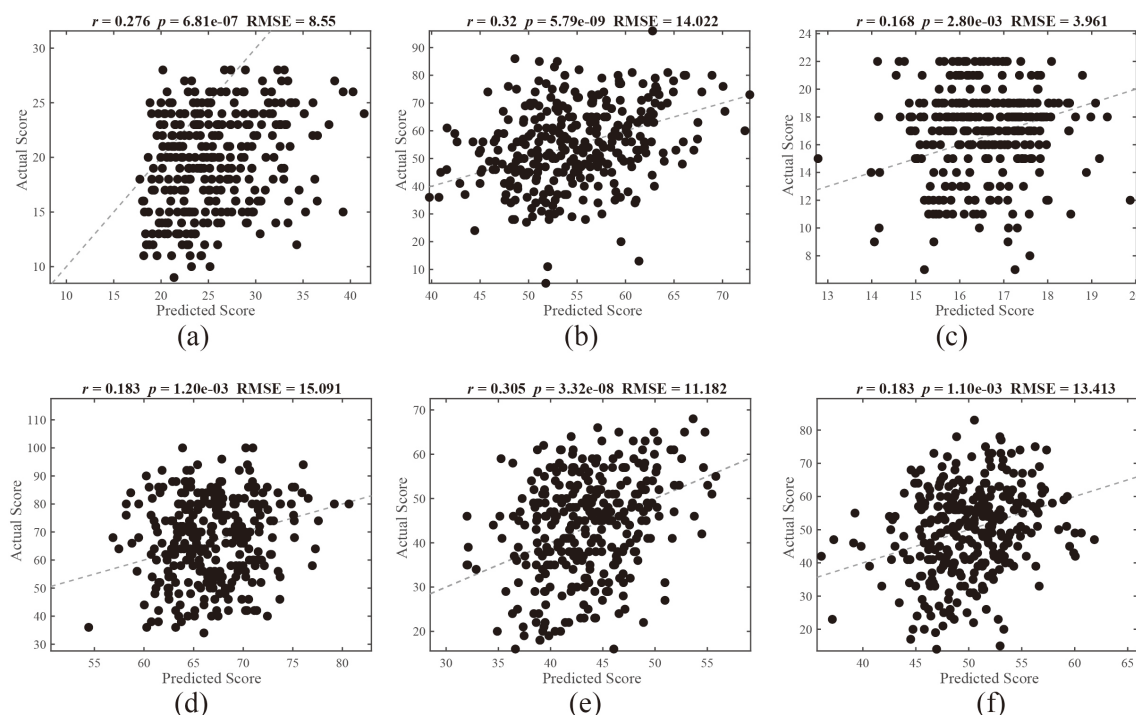


Figure 3.8 Relationship between actual and predicted scores on each cognitive task (by Pearson correlation). (a) Digit sequencing task; (b) Symbol-coding task; (c) Tower of London task; (d) Token motor task; (e) Animal naming task; (f) Verbal memory scores.

3.6 Discussion

Previous studies have found that schizophrenia has varying degrees of impairment in cognitive function and cerebral cortex compared to healthy individuals. In the present study, researchers found that SCZ patients scored lower than healthy subjects on the tasks of digit sequencing task, symbol-coding, Tower of London, token motor, verbal memory, and animal naming. This suggests impairments of SCZ in neurocognitive functions such as working memory (Lee & Park, 2005), processing speed, attention, planning and

execution ability, motor control, and verbal (Brébion, David, Bressan, & Pilowsky, 2006), and memory abilities, respectively. Our results are consistent with previous studies and we both found significantly lower scores on various BACS tasks in SCZ patients (Keefe et al., 2008). Neurocognitive deficits are one of the most important features of psychiatric syndromes. In fact, functional imaging is closely related to cognitive deficits which can provide guidance for cognitive intervention and rehabilitation. In this thesis, we explored the differences in ERP and brain network dynamics between SCZ patients and healthy controls and their relationship with neurocognitive dysfunction to provide new insight for the exploration of neurophysiological endophenotypes.

First, the P300 mainly reflects extensive synchronization between the prefrontal and parietal cortex, reflecting the involvement of higher cognitive processes such as attention, working memory, cognitive control, and decision-making. Besides, P300 is associated with information processing deficits and thus has been used in studies of schizophrenia. In the present study, we found significant differences between SCZ patients and healthy controls in the information processing states characterized by the P300. Indeed, a decrease in P300 amplitude is the most common and reproducible of psychotic phenotypes (Bramon et al., 2004). Previous studies have shown that the altered amplitude of the P300 in SCZ patients correlates with working memory capacity. Parker et al revealed strong correlations between P300 amplitude and cognitive abilities such as attention, planning and execution, and verbal ability (Parker et al., 2021). In the ERP study, our study is highly consistent with previous studies. The P300 component can characterize cognitive abilities in individuals with severe psychotic syndromes.

Furthermore, it has been previously clarified that schizophrenia is a brain disconnection disorder (Friston & Frith, 1995). SCZ patients have significant abnormalities in brain network dynamics. However, few have revealed the brain abnormalities of SCZ patients from the coupling of structural and functional signals. Thus, in this study, we mainly utilized the graph spectral theory to explore the altered EEG network dynamics in schizophrenia and its relationship with brain cognitive deficits. As shown in Figure 3.3, our results indicate that the overall GPSD of the SCZ patients was significantly reduced during P300 and that this change did not occur at a single harmonic, but was significantly reduced at both high-frequency and low-frequency harmonics. Previous studies have clarified that low-frequency graph harmonics correspond to long-range connectivity-related activity patterns, while high-frequency graph harmonics correspond more to short-

range connectivity patterns. The low-frequency and high-frequency graph harmonics are also believed to encode the two information processing modes of integration and segregation, respectively (Glomb et al., 2020; Rué-Queralt et al., 2021; Rué-Queralt et al., 2023; R. Wang et al., 2019). The alteration of GPSD in low-frequency and high-frequency graph harmonics during P300 reminds us that functional segregation and integration may be disrupted in SCZ patients compared to healthy controls. Studies have reported possible alterations in integration and segregation dynamics for SCZ patients by exploring the small-world properties of the network. The SCZ patients showed lower clustering (segregation metrics) and shorter path lengths (integration metrics) compared to the HC (Rubinov et al., 2009). Similarly, Vértes et al. found reduced topological properties of clustering and modularity in childhood-onset SCZ (Vértes et al., 2012). Our reports are consistent with the current findings. The reduction of the GPSD for SCZ patients and its strong correlation with neurocognition in Figure 3.5 suggests that the cortical dynamics of the SCZ patients slowed down, and the slowing down of flexibility affected the cognitive activity of the SCZ patients, leading to abnormal behavioral performance of the SCZ patients in various cognitive tasks.

To further investigate cortical temporal rhythmic alterations in SCZ patients at different spatial scales, we divided the signal into a graph low-frequency component that relies more on the graph structure and a high-frequency component that is more liberal relative to the graph structure. The results in Figure 3.4 show that differences in δ band are more likely captured by graph low-frequency harmonics compared to β and γ bands. The β and γ band differences are scattered in both high-frequency and low-frequency harmonics. Current research suggests that different temporal frequencies support different spatial scales of information processing patterns (Fries, 2015; Vezoli et al., 2021). Low-frequency oscillations are more inclined to modulate long-range interactions and high-frequency oscillations are more inclined to modulate short-range localized activity (Rué-Queralt et al., 2023). We can infer that the graph low-frequency harmonic captures long-range connectivity patterns and should be more inclined to capture the activity of low-frequency rhythms such as δ and θ bands. This is broadly consistent with the findings of this thesis. However, the present differences of γ and β bands in both low-frequency and high-frequency graph harmonics in this thesis may be influenced by the order of graph filter. In addition, the results in Figure 3.4 further illustrate that the four graph low-frequency connectome harmonics are sufficient to capture most of the difference patterns

of temporal rhythm between SCZ patients and HC, proving the reliability of dimensionality reduction and the graph spectral filters with graph harmonics.

In addition, in this thesis, we found that the activation in the δ -band captured by the graph low-frequency harmonics significantly decreased in the frontal and temporal, and occipital lobes. Indeed, studies of anatomical findings have reported gray matter atrophy in frontal, temporal, thalamic, and occipital regions in SCZ patients (Andreasen et al., 2011; Hu et al., 2020; Tesli et al., 2020), as well as diminished activation in the δ -band (Schmiedt et al., 2005). The results in this thesis are highly consistent with the current findings. In order to further validate the relationship between cognitive abilities and the activation patterns in δ -band captured by the low-frequency graph harmonics, we predicted the subjects' cognitive task scores with the PSD in the temporal and prefrontal lobes in δ -band. The result is shown in Figure 3.8. Consistent with the correlation results as shown in Figure 3.6, the PSD of δ -band can better predict the scores of symbol-coding and verbal memory compared to the other four tasks. This may indicate that the high degree of frontal and temporal gray matter atrophy in the SCZ patients prevented the SCZ patients from the maintenance of the normal activity of corresponding EEG rhythms during the P300 process and further affected the neurocognitive abilities of SCZ patients, especially attention, processing speed, and verbal memory abilities (Donati, D'Agostino, & Ferrarelli, 2020). Compared to the gamma rhythm, the δ and θ rhythms are the main components of P300. The difference in the δ rhythm further validates the induced P300 may be caused by abnormalities in the frontal, temporal, and occipital lobes.

Overall, our results reveal the changes in brain activation at different spatial scales of graph harmonics and reflect abnormal slowing down of brain network dynamics in SCZ patients as well as abnormal changes in EEG rhythms supported by different graph harmonics. These abnormal alterations are closely associated with neurocognitive deficits in SCZ patients, which provides some rationale for exploring the neural mechanisms and developing diagnostic techniques for SCZ patients.

3.7 Conclusion

In this section, we focus on the analysis and application of graph spectral theory in schizophrenia, exploring changes in the brain dynamics of SCZ patients, mainly with the help of harmonic energy as well as the activation of different brain rhythms at different spatial scales of graph harmonics in the SCZ patients. We explored the link between these

changes and neurocognitive deficits. In the present study, we found that changes in cortical dynamics of SCZ patients were slowed down, and that slowed flexibility led to impairments in numerous cognitive abilities. In addition, functional separation and integration may be disrupted in SCZ patients compared to healthy subjects. Besides, brain regions with differential activation in the δ -band were more compatible with the gray matter-reduced regions of SCZ patients, and the PSD of these regions was highly correlated with cognitive ability. The strong correlation between the brain network dynamics features captured by graph harmonics and cognitive abilities illustrates the difference in neural mechanisms between SCZ patients and healthy controls. It may provide new insight for the development of future diagnostic techniques for SCZ patients.

Chapter 4 General Discussion

4.1 Key Findings and Significance

Traditional time-frequency analysis techniques are insufficient to support us in decoding brain activity. Thus, the development of complex network analysis methods is important for understanding of cognitive neural mechanisms and development of diagnostic models of psychiatric and neurological disorders. Graph spectral theory is an emerging method and important tool for complex network analysis, which is now widely used in brain network disorders of psychiatric and neurological diseases, denoising FMRI, and function-structure coupling features. Functional network disorders in various psychiatric and neurological disorders like schizophrenia, ADHD, and Parkinson's have been widely reported in EEG studies. At present, researchers have less research on graph spectral theory in denoising and coupling of structural and functional signals, especially in EEG. On the one hand, unlike the traditional denoising techniques, the graph spectral theory is based on the invariance of the underlying structure of the signal, which fully takes into account the dependence between different brain regions and may be more in line with the mechanism of the brain itself. On the other hand, in the research of schizophrenia and other disorders, there are few studies that have explored the altered dynamics of the brain network in SCZ patients from the perspective of structural connectivity harmonics, and our study may fill the gap for this part of research exploration. In fact, brain function abnormalities of SCZ patients may be reflected in different connectivity harmonics, and the study of harmonics may be as important as the exploration of EEG rhythms. Based on this, in this thesis, we have successively focused on the application of graph spectral theory in denoising EEG and the graph spectral features of SZC, in order to develop more reliable denoising algorithms and conduct more in-depth research on the exploration of neural mechanisms and neurophysiological endophenotypes of SCZ. The results of this thesis are summarized as follows:

1. Based on the joint time-vertex framework, we develop a JFT graph based on the constraints of time smoothing and graph smoothing under the joint l_{pq} norm. To verify the robustness of the algorithm to different noises, we introduce impulse noise simulated by alpha-stable distributions, Gaussian noise, and resting EEG noise and explore the effect of JFT in real applications. We found that: (1) As the estimation of the graph

structure with the algorithm this thesis used will be affected by the quality of the EEG signal itself, GFT (only with graph smoothing) can't achieve denoising when the signal is seriously damaged. However, after DFT (only the time constraints) to improve the SNR ratio of the signal, GFT can further play a role, which makes JFT perform significantly better than that of the traditional wavelet, DFT, and GFT in denoising. JFT shows a good suppression ability for all three types of noise. (2) Further to verify the applicability of JFT, we used JFT as a preprocessing algorithm and found an improvement in the classification accuracy of EEG signals from healthy controls and SCZ patients and an improvement in the decoding efficiency of the brain-computer interface of the P300 spelling system. These results demonstrate the effectiveness of the JFT framework for filtering and our research can further promote the development of EEG denoising technology.

2. We then explored the graph spectral features of schizophrenia based on the oddball paradigm of the P300 to understand the altered brain dynamics of SCZ patients and their relationship with cognition. Based on this, we found: (1) a decrease in the P300 amplitude of the scalp EEG in SCZ patients; (2) abnormal energy changes at different harmonics in SCZ patients. On the one hand, the decrease in total GPSD indicates the slowing down of cortical dynamics in SCZ patients and affects their neurocognition; on the other hand, the balance between dissociation and integration in SCZ patients is disrupted which is reflected in the significant changes of different harmonic energies for SCZ patients; (3) most of the differential features of EEG rhythms in SCZ patients are captured by the low-frequency aligned signals and the δ -band in the aligned signals captured abnormal PSD activation in the SCZ patients in prefrontal, temporal, and occipital regions. This may be due to the fact that the normal activity in the δ -band is affected by the diminished gray matter volume of the SCZ patients over these regions, and the positive correlation between this abnormal change and cognitive performance further suggests that the abnormal activation in the δ -band affects the neurocognitive function of the SCZ patients. These results suggest that there are abnormal brain dynamics changes in SCZ patients during P300, and contribute to our understanding of the neural mechanisms of SCZ and provide new ideas for clinical diagnosis and treatment of SCZ patients.

4.2 Future Research

In this thesis, we have developed denoising and analysis methods for EEG based on graph spectral theory and have achieved some results so far. In the following, the limitations of the two current research works and the future research direction and content will be explained in detail.

1. In the denoising algorithm, this thesis uses the k-neighborhood algorithm to estimate the adjacency matrix, which relies on the EEG signals and is not based on the true structural distances. So GFT based on the graph structure is susceptible to the interference of the noise, which will lead to the failure of the graph filters when the noise causes a large change in the signal. In this regard, future denoising algorithms of EEG can conduct in-depth research on the graph structure itself.

2. In addition, the filters in this thesis emphasize constraints based on simultaneous time and graph. Regarding the simultaneous constraints on time and graph space, we mainly consider the smoothness constraints, but in fact, more constraint strategies can be introduced into the framework, such as graph wavelet filters and Slepian operators which can suppress excessive signal energy at some nodes.

3. In the direction of exploring the brain network dynamics of schizophrenia based on graph spectral theory, we did not deeply explore the differences in each harmonic of SCZ patients but divided the harmonics into 10 groups. In fact, each harmonic may be as worthy of deeper exploration as the EEG rhythms. The delineation of harmonic rhythms may later be as important to cognitive research as the delineation of EEG rhythms.

4. In addition, changes in brain dynamics regarding the SCZ during different specific cognitive processing could be also considered in the future. In this process, we have focused on neural processes in the oddball paradigm and have not focused on cognitive changes in the brain during other cognitive processing, such as working memory load. In future studies, the analytical ideas presented in this thesis can also be applied to the brain state changes in the coupling of structural and functional signals in healthy controls and SCZ patients in the study of cognitive tasks such as working memory.

5. In this thesis, we lack further analysis on whether the characteristics captured by the research methods are heritable. Besides, this thesis did not gain access to the DTI of SCZ patients for the construction of the graph harmonics for each subject but rather used the 13% of the strongest connections in healthy controls. However, the consistency of the coupling of EEG rhythms and graph harmonics with the current research can still indicate

the validity of the analysis techniques presented in this thesis. In the subsequent work, we will collect the DTI data of both SCZ patients, and study the alterations in the structural graph harmonics of the two groups, as well as the coupling characteristics of the functional signals with the structural graph harmonics to find out the relationship between cognitive alterations and the functional brain states. In addition, to further validate whether the proposed method can truly serve as a biomarker for SCZ, we will further collect data from first-degree relatives of SCZ patients to verify the alterations in the brain states compared to healthy subjects and SCZ patients and to find similar features between the relatives and SCZ patients, as well as the links between these brain features and the genetic profiles.

Chapter 5 Bibliography

- Abi-Dargham, A., Javitch, J. A., Slifstein, M., Anticevic, A., Calkins, M. E., Cho, Y. T., . . . Gur, R. E. (2022). Dopamine D1R receptor stimulation as a mechanistic pro-cognitive target for schizophrenia. *Schizophrenia bulletin*, *48*(1), 199-210.
- Abramian, D., Larsson, M., Eklund, A., Aganj, I., Westin, C.-F., & Behjat, H. (2021). Diffusion-informed spatial smoothing of fMRI data in white matter using spectral graph filters. *NeuroImage*, *237*, 118095.
- Alyasserri, Z. A. A., Khader, A. T., Al-Betar, M. A., Abasi, A. K., & Makhadmeh, S. N. (2019). EEG signals denoising using optimal wavelet transform hybridized with efficient metaheuristic methods. *IEEE Access*, *8*, 10584-10605.
- Amzica, F., & Steriade, M. (1998). Electrophysiological correlates of sleep delta waves. *Electroencephalography and clinical neurophysiology*, *107*(2), 69-83.
- An, Y., Lam, H. K., & Ling, S. H. (2022). Auto-Denoising for EEG Signals Using Generative Adversarial Network. *Sensors*, *22*(5), 1750.
- Andreasen, N. C., Nopoulos, P., Magnotta, V., Pierson, R., Ziebell, S., & Ho, B.-C. (2011). Progressive brain change in schizophrenia: a prospective longitudinal study of first-episode schizophrenia. *Biological psychiatry*, *70*(7), 672-679.
- Antonova, E., Sharma, T., Morris, R., & Kumari, V. (2004). The relationship between brain structure and neurocognition in schizophrenia: a selective review. *Schizophrenia research*, *70*(2-3), 117-145.
- Atasoy, S., Roseman, L., Kaelen, M., Kringelbach, M. L., Deco, G., & Carhart-Harris, R. L. (2017). Connectome-harmonic decomposition of human brain activity reveals dynamical repertoire reorganization under LSD. *Scientific reports*, *7*(1), 17661.
- Ayano, G., Demelash, S., Yohannes, Z., Haile, K., Tulu, M., Assefa, D., . . . Chaka, A. (2021). Misdiagnosis, detection rate, and associated factors of severe psychiatric disorders in specialized psychiatry centers in Ethiopia. *Annals of general psychiatry*, *20*, 1-10.
- Başar, E., & Güntekin, B. (2008). A review of brain oscillations in cognitive disorders and the role of neurotransmitters. *Brain research*, *1235*, 172-193.
- Basharpoor, S., Heidari, F., & Molavi, P. (2021). EEG coherence in theta, alpha, and beta bands in frontal regions and executive functions. *Applied Neuropsychology: Adult*, *28*(3), 310-317.

- Behjat, H., Westin, C.-F., & Aganj, I. (2021). *Cortical surface-informed volumetric spatial smoothing of fMRI data via graph signal processing*. Paper presented at the 2021 43rd Annual International Conference of the IEEE Engineering in Medicine & Biology Society (EMBC), Mexico.
- Bohlin, T. (1977). Analysis of EEG signals with changing spectra using a short-word Kalman estimator. *Mathematical Biosciences*, 35(3-4), 221-259.
- Borowicz, A. (2018). Using a multichannel Wiener filter to remove eye-blink artifacts from EEG data. *Biomedical Signal Processing and Control*, 45, 246-255.
- Brahim, A., Hajjam El Hassani, M., & Farrugia, N. (2019). *Classification of autism spectrum disorder through the graph fourier transform of fmri temporal signals projected on structural connectome*. Paper presented at the Computer Analysis of Images and Patterns: CAIP 2019 International Workshops, Salerno, Italy.
- Bramon, E., Rabe-Hesketh, S., Sham, P., Murray, R. M., & Frangou, S. (2004). Meta-analysis of the P300 and P50 waveforms in schizophrenia. *Schizophrenia research*, 70(2-3), 315-329.
- Brébion, G., David, A. S., Bressan, R. A., & Pilowsky, L. S. (2006). Processing speed: a strong predictor of verbal memory performance in schizophrenia. *Journal of Clinical and Experimental Neuropsychology*, 28(3), 370-382.
- Buchsbaum, M. S., Christian, B. T., Lehrer, D. S., Narayanan, T. K., Shi, B., Mantil, J., . . . Mukherjee, J. (2006). D2/D3 dopamine receptor binding with [F-18] fallypride in thalamus and cortex of patients with schizophrenia. *Schizophrenia research*, 85(1-3), 232-244.
- Buzsáki, G. (2002). Theta oscillations in the hippocampus. *Neuron*, 33(3), 325-340.
- Carlsson, A., & Lindqvist, M. (1963). Effect of chlorpromazine or haloperidol on formation of 3 - methoxytyramine and normetanephrine in mouse brain. *Acta pharmacologica et toxicologica*, 20(2), 140-144.
- Carlton, E. H., & Katz, S. (1980). Is Wiener filtering an effective method of improving evoked potential estimation? *IEEE Transactions on Biomedical Engineering*(4), 187-192.
- Carmona, R. A., & Hudgins, L. H. (1994). *Wavelet denoising of EEG signals and identification of evoked response potentials*. Paper presented at the Wavelet Applications in Signal and Image Processing II, San Diego, CA, United States.
- Castellanos, F. X., Margulies, D. S., Kelly, C., Uddin, L. Q., Ghaffari, M., Kirsch, A., . . . Biswal, B. (2008). Cingulate-precuneus interactions: a new locus of dysfunction in adult attention-deficit/hyperactivity disorder. *Biological psychiatry*, 63(3), 332-337.
- Chapman, R. M., & McCrary, J. W. (1995). EP component identification and measurement by principal components-analysis. *Brain and cognition*, 27(3), 288-310.

- Chen, X., Xu, X., Liu, A., McKeown, M. J., & Wang, Z. J. (2017). The use of multivariate EMD and CCA for denoising muscle artifacts from few-channel EEG recordings. *IEEE Transactions on Instrumentation and Measurement*, 67(2), 359-370.
- Chuang, C.-H., Chang, K.-Y., Huang, C.-S., & Jung, T.-P. (2022). IC-U-Net: a U-Net-based denoising autoencoder using mixtures of independent components for automatic EEG artifact removal. *NeuroImage*, 263, 119586.
- Clementz, B. A., Sweeney, J. A., Hamm, J. P., Ivleva, E. I., Ethridge, L. E., Pearlson, G. D., . . . Tamminga, C. A. (2016). Identification of distinct psychosis biotypes using brain-based biomarkers. *American Journal of Psychiatry*, 173(4), 373-384.
- Condat, L. (2013). A direct algorithm for 1-D total variation denoising. *IEEE Signal Processing Letters*, 20(11), 1054-1057.
- Coyle, J. T. (2006). Glutamate and schizophrenia: beyond the dopamine hypothesis. *Cellular and molecular neurobiology*, 26, 363-382.
- Creese, I., Burt, D. R., & Snyder, S. H. (1976). Dopamine receptor binding predicts clinical and pharmacological potencies of antischizophrenic drugs. *Science*, 192(4238), 481-483.
- Csernansky, J. G., & Cronenwett, W. J. (2008). Neural networks in schizophrenia. In (Vol. 165, pp. 937-939): American Journal of Psychiatry.
- Da Silva, F. L. J. E., Lippincott Williams, & Wilkins, P. (1999). Event-related potentials: methodology and quantification. *Electroencephalography, Lippincott Williams and Wilkins, Philadelphia*.
- Davis, K. L., Kahn, R. S., Ko, G., & Davidson, M. (1991). Dopamine in schizophrenia: a review and reconceptualization. *The American journal of psychiatry*, 148(11), 1474-1486.
- De Clercq, W., Vergult, A., Vanrumste, B., Van Paesschen, W., & Van Huffel, S. (2006). Canonical correlation analysis applied to remove muscle artifacts from the electroencephalogram. *IEEE Transactions on Biomedical Engineering*, 53(12), 2583-2587.
- DeLisi, L. E., Sakuma, M., Kushner, M., Finer, D. L., Hoff, A. L., & Crow, T. J. (1997). Anomalous cerebral asymmetry and language processing in schizophrenia. *Schizophrenia bulletin*, 23(2), 255-271.
- Donati, F. L., D'Agostino, A., & Ferrarelli, F. (2020). Neurocognitive and neurophysiological endophenotypes in schizophrenia: An overview. *Biomarkers in Neuropsychiatry*, 3, 100017.
- Donchin, E., Spencer, K. M., & Wijesinghe, R. (2000). The mental prosthesis: assessing the speed of a P300-based brain-computer interface. *IEEE transactions on rehabilitation engineering*, 8(2), 174-179.

- Dongwei, C., Fang, W., Zhen, W., Haifang, L., & Junjie, C. (2013). *EEG-based emotion recognition with brain network using independent components analysis and granger causality*. Paper presented at the 2013 International Conference on Computer Medical Applications (ICCMA), Sousse, Tunisia.
- Donoho, D. L., & Johnstone, I. M. (1994). Ideal spatial adaptation by wavelet shrinkage. *Biometrika*, *81*(3), 425-455.
- Donoho, D. L., & Johnstone, I. M. (1995). Adapting to unknown smoothness via wavelet shrinkage. *Journal of the american statistical association*, *90*(432), 1200-1224.
- Dora, M., & Holcman, D. (2022). Adaptive single-channel EEG artifact removal with applications to clinical monitoring. *IEEE Transactions on Neural Systems and Rehabilitation Engineering*, *30*, 286-295.
- Einizade, A., & Sardouie, S. H. (2022). A unified approach for simultaneous graph learning and blind separation of graph signal sources. *IEEE Transactions on Signal and Information Processing over Networks*, *8*, 543-555.
- Ellison-Wright, I., & Bullmore, E. (2009). Meta-analysis of diffusion tensor imaging studies in schizophrenia. *Schizophrenia research*, *108*(1-3), 3-10.
- Eryilmaz, H., Pax, M., O'Neill, A. G., Vangel, M., Diez, I., Holt, D. J., . . . Roffman, J. L. (2022). Network hub centrality and working memory performance in schizophrenia. *Schizophrenia*, *8*(1), 76.
- Fadili, M.-J., & Starck, J.-L. (2009). *Monotone operator splitting for optimization problems in sparse recovery*. Paper presented at the 2009 16th IEEE International Conference on Image Processing (ICIP), Cairo, Egypt.
- Farwell, L. A., & Donchin, E. (1988). Talking off the top of your head: toward a mental prosthesis utilizing event-related brain potentials. *Electroencephalography and clinical neurophysiology*, *70*(6), 510-523.
- Farzan, F., Barr, M. S., Levinson, A. J., Chen, R., Wong, W., Fitzgerald, P. B., & Daskalakis, Z. J. (2010). Evidence for gamma inhibition deficits in the dorsolateral prefrontal cortex of patients with schizophrenia. *Brain*, *133*(5), 1505-1514.
- Fassbender, C., Zhang, H., Buzy, W. M., Cortes, C. R., Mizuri, D., Beckett, L., & Schweitzer, J. B. (2009). A lack of default network suppression is linked to increased distractibility in ADHD. *Brain research*, *1273*, 114-128.
- Ferrillo, F., Beelke, M., & Nobili, L. (2000). Sleep EEG synchronization mechanisms and activation of interictal epileptic spikes. *Clinical Neurophysiology*, *111*, S65-S73.

- Fries, P. (2015). Rhythms for cognition: communication through coherence. *Neuron*, 88(1), 220-235.
- Friston, K. J., & Frith, C. D. (1995). Schizophrenia: a disconnection syndrome. *Clin Neurosci*, 3(2), 89-97.
- Gaur, P., Gupta, H., Chowdhury, A., McCreadie, K., Pachori, R. B., & Wang, H. (2021). A sliding window common spatial pattern for enhancing motor imagery classification in EEG-BCI. *IEEE Transactions on Instrumentation and Measurement*, 70, 1-9.
- Georgiadis, K., Adamos, D. A., Nikolopoulos, S., Laskaris, N., & Kompatsiaris, I. (2021). Covariation informed graph sLepians for motor imagery decoding. *IEEE Transactions on Neural Systems and Rehabilitation Engineering*, 29, 340-349.
- Georgiadis, K., Laskaris, N., Nikolopoulos, S., & Kompatsiaris, I. (2019). Connectivity steered graph Fourier transform for motor imagery BCI decoding. *Journal of neural engineering*, 16(5), 056021.
- Glomb, K., Kringelbach, M. L., Deco, G., Hagmann, P., Pearson, J., & Atasoy, S. (2021). Functional harmonics reveal multi-dimensional basis functions underlying cortical organization. *Cell Reports*, 36(8).
- Glomb, K., Queralt, J. R., Pascucci, D., Defferrard, M., Tourbier, S., Carboni, M., . . . Hagmann, P. (2020). Connectome spectral analysis to track EEG task dynamics on a subsecond scale. *NeuroImage*, 221, 117137.
- Grassi, F., Loukas, A., Perraudin, N., & Ricaud, B. (2017). A time-vertex signal processing framework: Scalable processing and meaningful representations for time-series on graphs. *IEEE Transactions on Signal Processing*, 66(3), 817-829.
- Gratton, C., Koller, J. M., Shannon, W., Greene, D. J., Maiti, B., Snyder, A. Z., . . . Campbell, M. C. (2019). Emergent functional network effects in Parkinson disease. *Cerebral Cortex*, 29(6), 2509-2523.
- Gur, R. E., Calkins, M. E., Gur, R. C., Horan, W. P., Nuechterlein, K. H., Seidman, L. J., & Stone, W. S. (2007). The consortium on the genetics of schizophrenia: neurocognitive endophenotypes. *Schizophrenia bulletin*, 33(1), 49-68.
- Hacker, C. D., Perlmutter, J. S., Criswell, S. R., Ances, B. M., & Snyder, A. Z. (2012). Resting state functional connectivity of the striatum in Parkinson's disease. *Brain*, 135(12), 3699-3711.
- Helmich, R. C., Derikx, L. C., Bakker, M., Scheeringa, R., Bloem, B. R., & Toni, I. (2010). Spatial remapping of cortico-striatal connectivity in Parkinson's disease. *Cerebral Cortex*, 20(5), 1175-1186.
- Hobbs, B., & Artemiadis, P. (2020). A review of robot-assisted lower-limb stroke therapy: unexplored paths and future directions in gait rehabilitation. *Frontiers in neurobotics*, 14, 19.

- Howes, O. D., Montgomery, A. J., Asselin, M.-C., Murray, R. M., Valli, I., Tabraham, P., . . . Broome, M. (2009). Elevated striatal dopamine function linked to prodromal signs of schizophrenia. *Archives of general psychiatry*, *66*(1), 13-20.
- Hu, N., Luo, C., Zhang, W., Yang, X., Xiao, Y., Sweeney, J. A., . . . Gong, Q. (2020). Hippocampal subfield alterations in schizophrenia: a selective review of structural MRI studies. *Biomarkers in Neuropsychiatry*, *3*, 100026.
- Hyvärinen, A., & Oja, E. (1997). A fast fixed-point algorithm for independent component analysis. *Neural computation*, *9*(7), 1483-1492.
- Jalili, M., & Knyazeva, M. G. (2011). EEG-based functional networks in schizophrenia. *Computers in Biology*, *41*(12), 1178-1186.
- Jestrović, I., Coyle, J. L., & Sejdić, E. (2017). Differences in brain networks during consecutive swallows detected using an optimized vertex–frequency algorithm. *Neuroscience*, *344*, 113-123.
- Jiang, Y., Luo, C., Li, X., Duan, M., He, H., Chen, X., . . . Woelfer, M. (2018). Progressive reduction in gray matter in patients with schizophrenia assessed with MR imaging by using causal network analysis. *Radiology*, *287*(2), 633-642.
- Jung, H.-T., Kim, D.-W., Kim, S., Im, C.-H., & Lee, S.-H. (2012). Reduced source activity of event-related potentials for affective facial pictures in schizophrenia patients. *Schizophrenia research*, *136*(1-3), 150-159.
- Jung, T.-P., Humphries, C., Lee, T.-W., Makeig, S., McKeown, M., Iragui, V., & Sejnowski, T. J. (1997). Extended ICA removes artifacts from electroencephalographic recordings. *Advances in neural information processing systems*, *10*.
- Just, M. A., Cherkassky, V. L., Keller, T. A., Kana, R. K., & Minshew, N. J. (2007). Functional and anatomical cortical underconnectivity in autism: evidence from an fMRI study of an executive function task and corpus callosum morphometry. *Cerebral Cortex*, *17*(4), 951-961.
- Kalantar, G., Sadreazami, H., Mohammadi, A., & Asif, A. (2017). *Adaptive dimensionality reduction method using graph-based spectral decomposition for motor imagery-based brain-computer interfaces*. Paper presented at the 2017 IEEE Global Conference on Signal and Information Processing (GlobalSIP), Montreal, QC, Canada.
- Kana, R. K., Keller, T. A., Cherkassky, V. L., Minshew, N. J., & Just, M. A. (2006). Sentence comprehension in autism: thinking in pictures with decreased functional connectivity. *Brain*, *129*(9), 2484-2493.

- Kane, J. M., Robinson, D. G., Schooler, N. R., Mueser, K. T., Penn, D. L., Rosenheck, R. A., . . . Estroff, S. E. (2016). Comprehensive versus usual community care for first-episode psychosis: 2-year outcomes from the NIMH RAISE early treatment program. *American Journal of Psychiatry*, *173*(4), 362-372.
- Karlsson, P., Farde, L., Halldin, C., & Sedvall, G. (2002). PET study of D1 dopamine receptor binding in neuroleptic-naive patients with schizophrenia. *American Journal of Psychiatry*, *159*(5), 761-767.
- Kedzior, B.-E. C. A. H., & KMathes, B. (2007). Working memory related gamma oscillations in schizophrenia patients. *Int J Psychophysiol*, *64*, 3945.
- Keefe, R. S., Harvey, P. D., Goldberg, T. E., Gold, J. M., Walker, T. M., Kennel, C., & Hawkins, K. (2008). Norms and standardization of the Brief Assessment of Cognition in Schizophrenia (BACS). *Schizophrenia research*, *102*(1-3), 108-115.
- Kestler, L., Walker, E., & Vega, E. (2001). Dopamine receptors in the brains of schizophrenia patients: a meta-analysis of the findings. *Behavioural pharmacology*, *12*(5), 355-371.
- Khatwani, P., & Tiwari, A. (2013). A survey on different noise removal techniques of EEG signals. *International Journal of Advanced Research in Computer and Communication Engineering*, *2*(2), 1091-1095.
- Kidogami, Y., Yoneda, H., Asaba, H., & Sakai, T. (1991). P300 in first degree relatives of schizophrenics. *Schizophrenia research*, *6*(1), 9-13.
- La Vaque, T. (1999). The history of EEG hans berger: psychophysiological. A historical vignette. *Journal of Neurotherapy*, *3*(2), 1-9.
- Lee, J., & Park, S. (2005). Working memory impairments in schizophrenia: a meta-analysis. *Journal of abnormal psychology*, *114*(4), 599.
- Levy, D. L., O'Driscoll, G., Matthyse, S., Cook, S. R., Holzman, P. S., & Mendell, N. R. (2004). Antisaccade performance in biological relatives of schizophrenia patients: a meta-analysis. *Schizophrenia research*, *71*(1), 113-125.
- Li, C., Li, P., Zhang, Y., Li, N., Si, Y., Li, F., . . . Systems, L. (2023). Effective emotion recognition by learning discriminative graph topologies in EEG brain networks. *IEEE Transactions on Neural Networks and Learning Systems*.
- Li, J., Wu, G.-R., Shi, M., Xia, J., Meng, Y., Yang, S., . . . Liao, W. (2023). Spatiotemporal topological correspondence between blood oxygenation and glucose metabolism revealed by simultaneous fPET-fMRI in brain's white matter. *Cerebral Cortex*, *33*(15), bhad201.

- Li, P., Gao, X., Li, C., Yi, C., Huang, W., Si, Y., . . . Systems, L. (2023). Granger causal inference based on dual laplacian distribution and its application to MI-BCI classification. *IEEE Transactions on Neural Networks and Learning Systems*.
- Li, R., Yuan, X., Radfar, M., Marendy, P., Ni, W., O'Brien, T. J., & Casillas-Espinosa, P. M. (2021). Graph signal processing, graph neural network and graph learning on biological data: a systematic review. *IEEE Reviews in Biomedical Engineering*, *16*, 109-135.
- Li, Y., & Mateos, G. (2019). *Identifying structural brain networks from functional connectivity: A network deconvolution approach*. Paper presented at the ICASSP 2019-2019 IEEE International Conference on Acoustics, Speech and Signal Processing (ICASSP), Brighton, UK.
- Lieberman, J., Kane, J., & Alvir, J. (1987). Provocative tests with psychostimulant drugs in schizophrenia. *Psychopharmacology*, *91*, 415-433.
- Light, G. A., Hsu, J. L., Hsieh, M. H., Meyer-Gomes, K., Sprock, J., Swerdlow, N. R., & Braff, D. L. (2006). Gamma band oscillations reveal neural network cortical coherence dysfunction in schizophrenia patients. *Biological psychiatry*, *60*(11), 1231-1240.
- Liu, Y., Liang, M., Zhou, Y., He, Y., Hao, Y., Song, M., . . . Jiang, T. (2008). Disrupted small-world networks in schizophrenia. *Brain*, *131*(4), 945-961.
- Luppi, A. I., Vohryzek, J., Kringelbach, M. L., Mediano, P. A., Craig, M. M., Adapa, R., . . . Peattie, A. R. (2023). Distributed harmonic patterns of structure-function dependence orchestrate human consciousness. *Communications biology*, *6*(1), 117.
- Makeig, S., Bell, A., Jung, T.-P., & Sejnowski, T. J. (1995). Independent component analysis of electroencephalographic data. *Advances in neural information processing systems*, *8*.
- Markovic, A., Kaess, M., & Tarokh, L. (2020). Gender differences in adolescent sleep neurophysiology: a high-density sleep EEG study. *Scientific reports*, *10*(1), 15935.
- Mashhadi, N., Khuzani, A. Z., Heidari, M., & Khaledyan, D. (2020). *Deep learning denoising for EOG artifacts removal from EEG signals*. Paper presented at the 2020 IEEE Global Humanitarian Technology Conference (GHTC), Seattle, WA, USA.
- McGowan, S., Lawrence, A. D., Sales, T., Queded, D., & Grasby, P. (2004). Presynaptic dopaminergic dysfunction in schizophrenia: a positron emission tomographic [18F] fluorodopa study. *Archives of general psychiatry*, *61*(2), 134-142.
- McGrath, J., Saha, S., Chant, D., & Welham, J. (2008). Schizophrenia: a concise overview of incidence, prevalence, and mortality. *Epidemiologic reviews*, *30*(1), 67-76.

- Medaglia, J. D., Huang, W., Karuza, E. A., Kelkar, A., Thompson-Schill, S. L., Ribeiro, A., & Bassett, D. S. (2018). Functional alignment with anatomical networks is associated with cognitive flexibility. *Nature human behaviour*, 2(2), 156-164.
- Meyer-Lindenberg, A., Miletich, R. S., Kohn, P. D., Esposito, G., Carson, R. E., Quarantelli, M., . . . Berman, K. F. (2002). Reduced prefrontal activity predicts exaggerated striatal dopaminergic function in schizophrenia. *Nature neuroscience*, 5(3), 267-271.
- Morone, G., Paolucci, S., Cherubini, A., De Angelis, D., Venturiero, V., Coiro, P., & Iosa, M. (2017). Robot-assisted gait training for stroke patients: current state of the art and perspectives of robotics. *Neuropsychiatric disease and treatment*, 13, 1303-1311.
- Mowla, M. R., Ng, S.-C., Zilany, M. S., & Paramesran, R. (2015). Artifacts-matched blind source separation and wavelet transform for multichannel EEG denoising. *Biomedical Signal Processing and Control*, 22, 111-118.
- Naim-Feil, J., Rubinson, M., Freche, D., Grinshpoon, A., Peled, A., Moses, E., & Levit-Binnun, N. (2018). Altered brain network dynamics in schizophrenia: a cognitive electroencephalography study. *Biological Psychiatry: Cognitive Neuroscience and Neuroimaging*, 3(1), 88-98.
- Narayanan, B., O'Neil, K., Berwise, C., Stevens, M. C., Calhoun, V. D., Clementz, B. A., . . . Pearlson, G. D. (2014). Resting state electroencephalogram oscillatory abnormalities in schizophrenia and psychotic bipolar patients and their relatives from the bipolar and schizophrenia network on intermediate phenotypes study. *Biological psychiatry*, 76(6), 456-465.
- Okubo, Y., Suhara, T., Suzuki, K., Kobayashi, K., Inoue, O., Terasaki, O., . . . Matsushima, E. (1997). Decreased prefrontal dopamine D1 receptors in schizophrenia revealed by PET. *Nature*, 385(6617), 634-636.
- Ortega, A., Frossard, P., Kovačević, J., Moura, J. M., & Vandergheynst, P. (2018). Graph signal processing: Overview, challenges, and applications. *Proceedings of the IEEE*, 106(5), 808-828.
- Parker, D. A., Trotti, R. L., McDowell, J. E., Keedy, S. K., Hill, S. K., Gershon, E. S., . . . Tamminga, C. A. (2021). Auditory oddball responses across the schizophrenia-bipolar spectrum and their relationship to cognitive and clinical features. *American Journal of Psychiatry*, 178(10), 952-964.
- Pentari, A., Tzagkarakis, G., Marias, K., & Tsakalides, P. (2021). *Graph-based denoising of EEG signals in impulsive environments*. Paper presented at the 2020 28th European Signal Processing Conference (EUSIPCO), Amsterdam, Netherlands.
- Pentari, A., Tzagkarakis, G., Marias, K., & Tsakalides, P. (2022). Graph denoising of impulsive EEG signals and the effect of their graph representation. *Biomedical Signal Processing and Control*, 78, 103886.

- Petrovic, M., Bolton, T. A., Preti, M. G., Liégeois, R., & Van De Ville, D. (2019). Guided graph spectral embedding: Application to the *C. elegans* connectome. *Network Neuroscience*, 3(3), 807-826.
- Pilavci, Y. Y., & Farrugia, N. (2019). *Spectral graph wavelet transform as feature extractor for machine learning in neuroimaging*. Paper presented at the ICASSP 2019-2019 IEEE International Conference on Acoustics, Speech and Signal Processing (ICASSP), Brighton, UK.
- Polikoff, J. B., Bunnell, H. T., & Borkowski Jr, W. J. (1995). *Toward a P300-based computer interface*. Paper presented at the Proc. RESNA'95 Annual Conf., Vancouver, Canada.
- Preti, M. G., & Van De Ville, D. (2019). Decoupling of brain function from structure reveals regional behavioral specialization in humans. *Nature communications*, 10(1), 4747.
- Price, G., Cercignani, M., Parker, G. J., Altmann, D. R., Barnes, T. R., Barker, G. J., . . . Ron, M. A. (2008). White matter tracts in first-episode psychosis: a DTI tractography study of the uncinate fasciculus. *NeuroImage*, 39(3), 949-955.
- Repovs, G., Csernansky, J. G., & Barch, D. M. (2011). Brain network connectivity in individuals with schizophrenia and their siblings. *Biological psychiatry*, 69(10), 967-973.
- Rubinov, M., Knock, S. A., Stam, C. J., Micheloyannis, S., Harris, A. W., Williams, L. M., & Breakspear, M. (2009). Small - world properties of nonlinear brain activity in schizophrenia. *Human brain mapping*, 30(2), 403-416.
- Rudie, J. D., Shehzad, Z., Hernandez, L. M., Colich, N. L., Bookheimer, S. Y., Iacoboni, M., & Dapretto, M. (2012). Reduced functional integration and segregation of distributed neural systems underlying social and emotional information processing in autism spectrum disorders. *Cerebral Cortex*, 22(5), 1025-1037.
- Rué-Queralt, J., Glomb, K., Pascucci, D., Tourbier, S., Carboni, M., Vulliémoz, S., . . . Hagmann, P. (2021). The connectome spectrum as a canonical basis for a sparse representation of fast brain activity. *NeuroImage*, 244, 118611.
- Rué-Queralt, J., Mancini, V., Rochas, V., Latrèche, C., Uhlhaas, P. J., Michel, C. M., . . . Hagmann, P. (2023). The coupling between the spatial and temporal scales of neural processes revealed by a joint time-vertex connectome spectral analysis. *NeuroImage*, 280, 120337.
- Rui, L., Nejati, H., & Cheung, N.-M. (2016). *Dimensionality reduction of brain imaging data using graph signal processing*. Paper presented at the 2016 IEEE International Conference on Image Processing (ICIP), Phoenix, AZ, USA.
- Saboksayr, S. S., Mateos, G., & Cetin, M. (2021). Online discriminative graph learning from multi-class smooth signals. *Signal Processing*, 186, 108101.

- Sardouie, S. H., Albera, L., Shamsollahi, M. B., & Merlet, I. (2014). An efficient Jacobi-like deflationary ICA algorithm: application to EEG denoising. *IEEE Signal Processing Letters*, 22(8), 1198-1202.
- Schmiedt, C., Brand, A., Hildebrandt, H., & Basar-Eroglu, C. (2005). Event-related theta oscillations during working memory tasks in patients with schizophrenia and healthy controls. *Cognitive Brain Research*, 25(3), 936-947.
- Seeman, P., & Lee, T. (1975). Antipsychotic drugs: direct correlation between clinical potency and presynaptic action on dopamine neurons. *Science*, 188(4194), 1217-1219.
- Şendur, L., & Selesnick, I. W. (2002). *A bivariate shrinkage function for wavelet-based denoising*. Paper presented at the 2002 IEEE International Conference on Acoustics, Speech, and Signal Processing, Orlando, FL, USA.
- Şevik, A. E., Yağcıoğlu, A. E. A., Yağcıoğlu, S., Karahan, S., Gürses, N., & Yıldız, M. (2011). Neuropsychological performance and auditory event related potentials in schizophrenia patients and their siblings: a family study. *Schizophrenia research*, 130(1-3), 195-202.
- Sharma, T., Lancaster, E., Sigmundsson, T., Lewis, S., Takei, N., Gurling, H., . . . Murray, R. (1999). Lack of normal pattern of cerebral asymmetry in familial schizophrenic patients and their relatives—The Maudsley Family Study. *Schizophrenia research*, 40(2), 111-120.
- Shenton, M. E., Dickey, C. C., Frumin, M., & McCarley, R. W. (2001). A review of MRI findings in schizophrenia. *Schizophrenia research*, 49(1-2), 1-52.
- Shim, M., Hwang, H.-J., Kim, D.-W., Lee, S.-H., & Im, C.-H. (2016). Machine-learning-based diagnosis of schizophrenia using combined sensor-level and source-level EEG features. *Schizophrenia research*, 176(2-3), 314-319.
- Shuman, D. I., Narang, S. K., Frossard, P., Ortega, A., & Vandergheynst, P. (2013). The emerging field of signal processing on graphs: Extending high-dimensional data analysis to networks and other irregular domains. *IEEE Signal Processing Magazine*, 30(3), 83-98.
- Si, Y., Li, F., Duan, K., Tao, Q., Li, C., Cao, Z., . . . Yao, D. (2020). Predicting individual decision-making responses based on single-trial EEG. *NeuroImage*, 206, 116333.
- Sihag, S., Naze, S., Taghdiri, F., Gumus, M., Tator, C., Green, R., . . . Dominguez, L. G. (2022). Functional brain activity constrained by structural connectivity reveals cohort-specific features for serum neurofilament light chain. *Communications Medicine*, 2(1), 8.
- Sonuga-Barke, E. J., & Castellanos, F. X. (2007). Spontaneous attentional fluctuations in impaired states and pathological conditions: a neurobiological hypothesis. *Neuroscience and Biobehavioral Reviews*, 31(7), 977-986.

- Sparacino, G., Milani, S., Arslan, E., & Cobelli, C. (2002). A Bayesian approach to estimate evoked potentials. *Computer methods and programs in biomedicine*, *68*(3), 233-248.
- Sponheim, S. R., Clementz, B. A., Iacono, W. G., & Beiser, M. (1994). Resting EEG in first - episode and chronic schizophrenia. *Psychophysiology*, *31*(1), 37-43.
- Stotesbury, H., Kirkham, F. J., Kölbl, M., Balfour, P., Clayden, J. D., Sahota, S., . . . Kesse-Adu, R. (2018). White matter integrity and processing speed in sickle cell anemia. *Neurology*, *90*(23), e2042-e2050.
- Sutton, S., Braren, M., Zubin, J., & John, E. (1965). Evoked-potential correlates of stimulus uncertainty. *Science*, *150*(3700), 1187-1188.
- Swerdlow, N. R., Light, G. A., Sprock, J., Calkins, M. E., Green, M. F., Greenwood, T. A., . . . Nuechterlein, K. H. (2014). Deficient prepulse inhibition in schizophrenia detected by the multi-site COGS. *Schizophrenia research*, *152*(2-3), 503-512.
- Takahashi, H., Higuchi, M., & Suhara, T. (2006). The role of extrastriatal dopamine D2 receptors in schizophrenia. *Biological psychiatry*, *59*(10), 919-928.
- Tandon, R., Gaebel, W., Barch, D. M., Bustillo, J., Gur, R. E., Heckers, S., . . . Tsuang, M. (2013). Definition and description of schizophrenia in the DSM-5. *Schizophrenia research*, *150*(1), 3-10.
- Tarokh, L., Carskadon, M. A., & Achermann, P. (2010). Developmental changes in brain connectivity assessed using the sleep EEG. *Neuroscience*, *171*(2), 622-634.
- Tesli, N., van der Meer, D., Rokicki, J., Storvestre, G., Røsæg, C., Jensen, A., . . . Tesli, M. (2020). Hippocampal subfield and amygdala nuclei volumes in schizophrenia patients with a history of violence. *European archives of psychiatry and clinical neuroscience*, *270*, 771-782.
- Vértes, P. E., Alexander-Bloch, A. F., Gogtay, N., Giedd, J. N., Rapoport, J. L., & Bullmore, E. T. (2012). Simple models of human brain functional networks. *Proceedings of the National Academy of Sciences*, *109*(15), 5868-5873.
- Vezoli, J., Vinck, M., Bosman, C. A., Bastos, A. M., Lewis, C. M., Kennedy, H., & Fries, P. (2021). Brain rhythms define distinct interaction networks with differential dependence on anatomy. *Neuron*, *109*(23), 3862-3878. e3865.
- Wada, M., Kurose, S., Miyazaki, T., Nakajima, S., Masuda, F., Mimura, Y., . . . Mashima, Y. (2019). The P300 event-related potential in bipolar disorder: A systematic review and meta-analysis. *Journal of affective disorders*, *256*, 234-249.
- Wang, J., Dong, W., Li, Y., Wydell, T. N., Quan, W., Tian, J., . . . Yi, C. (2023). Discrimination of auditory verbal hallucination in schizophrenia based on EEG brain networks. *Psychiatry Research: Neuroimaging*, *331*, 111632.

- Wang, R., Lin, P., Liu, M., Wu, Y., Zhou, T., & Zhou, C. (2019). Hierarchical connectome modes and critical state jointly maximize human brain functional diversity. *Physical review letters*, *123*(3), 038301.
- Wang, Z.-M., Zhou, R., He, Y., & Guo, X.-M. (2020). Functional integration and separation of brain network based on phase locking value during emotion processing. *IEEE Transactions on Cognitive and Developmental Systems*, *15*(2), 444-453.
- Warren, N., Siskind, D., & O'Gorman, C. (2018). Refining the psychiatric syndrome of anti - N - methyl - d - aspartate receptor encephalitis. *Acta Psychiatrica Scandinavica*, *138*(5), 401-408.
- Wolpaw, J. R., McFarland, D. J., Vaughan, T. M., & Schalk, G. (2003). The Wadsworth Center brain-computer interface (BCI) research and development program. *IEEE Transactions on Neural Systems and Rehabilitation Engineering*, *11*(2), 1-4.
- Woo, T.-U. W., Walsh, J. P., & Benes, F. M. (2004). Density of glutamic acid decarboxylase 67 messenger rna-containing neurons that express the n-methyl-d-aspartate receptor subunit nr2a in the anterior cingulate cortex in schizophrenia and bipolar disorder. *Archives of General Psychiatry*, *61*(7), 649-657.
- Yan, W., Du, C., Wu, Y., Zheng, X., & Xu, G. (2021). SSVEP-EEG denoising via image filtering methods. *IEEE Transactions on Neural Systems and Rehabilitation Engineering*, *29*, 1634-1643.
- Yeragani, V. K., Cashmere, D., Miewald, J., Tancer, M., & Keshavan, M. S. (2006). Decreased coherence in higher frequency ranges (beta and gamma) between central and frontal EEG in patients with schizophrenia: a preliminary report. *Psychiatry research*, *141*(1), 53-60.
- Yurgelun-Todd, D. A., Coyle, J. T., Gruber, S. A., Renshaw, P. F., Silveri, M. M., Amico, E., . . . Goff, D. C. (2005). Functional magnetic resonance imaging studies of schizophrenic patients during word production: effects of D-cycloserine. *Psychiatry Research: Neuroimaging*, *138*(1), 23-31.
- Zalesky, A., Fornito, A., & Bullmore, E. T. (2010). Network-based statistic: identifying differences in brain networks. *NeuroImage*, *53*(4), 1197-1207.
- Zalesky, A., Fornito, A., Seal, M. L., Cocchi, L., Westin, C.-F., Bullmore, E. T., . . . Pantelis, C. (2011). Disrupted axonal fiber connectivity in schizophrenia. *Biological psychiatry*, *69*(1), 80-89.
- Zhang, H., Zhao, M., Wei, C., Mantini, D., Li, Z., & Liu, Q. (2021). EEGdenoiseNet: a benchmark dataset for deep learning solutions of EEG denoising. *Journal of neural engineering*, *18*(5), 056057.